Research Paper
Computational Methods for Differential Equations
http://cmde.tabrizu.ac.ir
Vol. 14, No. 2, 2026, pp. 519-548
DOI:10.22034/cmde.2025.64656.2935

Numerical approximation of coupled Schrödinger equations via NUAH B-spline DQM

Mamta Kapoor[1,*], **Geeta Arora**[2], **and Varun Joshi**[2]

[1]Marwadi University Research Center, Department of Mathematics, Faculty of Engineering and Technology, Marwadi University, Rajkot, 360003, Gujarat, India.

[2]Department of Mathematics, Lovely Professional University, Phagwara, Punjab, India-144411.

Abstract

The goal of the current study is to offer a novel method for numerically solving coupled $1D$ and $2D$ nonlinear Schrödinger equations. To discretize the spatial partial derivative, we applied the MCNUAH B-spline DQM. The SSP-RK43 technique is used to solve the reduced system of ODEs. Via the matrix method, the stability of the proposed method is investigated, and it is found to be stable. Four experiments are used to confirm the efficiency of the suggested scheme, and data from the literature are compared throughout. It is clear that the obtained results are satisfactory and in strong accord with preceding results. This approach yields superior outcomes and is effective, straightforward, and reasonably simple to use. The graphical abstract is provided as per Figure 1.

Keywords. Differential quadrature method, NUAH B-spline, SSP-RK43 scheme, Matrix stability method.

2010 Mathematics Subject Classification. 35Qxx, 34Axx, 37Mxx.

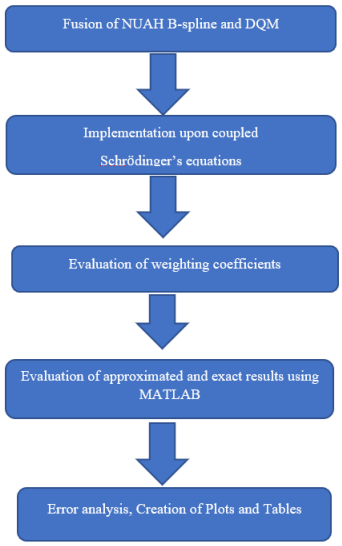

FIGURE 1. Graphical abstract.

Received: 23 Nobvember 2024; Accepted: 27 February 2025.
∗ Corresponding author. Email: mamtakapoor.78@yahoo.com.

1. Introduction

Various types of nonlinear Schrödinger equations expound on a wide variety of events with significant physical implications. The presented class of equations, referred to as the coupled Schrödinger equations, can be used to simulate a wide range of subjects in quantum fluids, condensed matter physics, nonlinear optics, gravitation, plasma physics, biological modeling, and many other domains.

(a) Coupled $1D$ Schrödinger equation. The 1D coupled Schrödinger equation is defined as follows:

$$i\left(\frac{\partial u}{\partial t}+\delta\frac{\partial u}{\partial x}\right)+\frac{1}{2}\frac{\partial^2 u}{\partial x^2}+\left(|u|^2+\epsilon|v|^2\right)u=0, \tag{1.1}$$

$$i\left(\frac{\partial v}{\partial t}-\delta\frac{\partial v}{\partial x}\right)+\frac{1}{2}\frac{\partial^2 v}{\partial x^2}+\left(\epsilon|u|^2+|v|^2\right)v=0, \tag{1.2}$$

where wave amplitudes for two polarizations are denoted by u and v, respectively, and normalized strength of linear birefringence is denoted by δ. According to Wadati et al. [66], the system of $1D$ Schrödinger equations (1.1) and (1.2) has the following exact solution:

$$u(x,t)=\sqrt{\frac{2\alpha}{1+\epsilon}}\,\operatorname{sech}\left[\sqrt{2\alpha}(x-\nu t)\right]\exp i\left[(\nu-\delta)x-\left(\frac{\nu^2-\delta^2}{2}-\alpha\right)t\right], \tag{1.3}$$

$$v(x,t)=\pm\sqrt{\frac{2\alpha}{1+\epsilon}}\,\operatorname{sech}\left[\sqrt{2\alpha}(x-\nu t)\right]\exp i\left[(\nu+\delta)x-\left(\frac{\nu^2-\delta^2}{2}-\alpha\right)t\right]. \tag{1.4}$$

Different interaction regimes would be studied in the present paper, and these interaction regimes will depend upon the values of δ and e, and along with the discussion of the interactions conserved quantities will also be studied. Two of the conserved quantities formulae are given as follows:

Mass conservation property:

$$I_1=\int_{-\infty}^{\infty}|u|^2\,dx, \tag{1.5}$$

$$I_2=\int_{-\infty}^{\infty}|v|^2\,dx. \tag{1.6}$$

(b) Coupled $2D$ Schrödinger equation. The coupled Schrödinger equation in two dimensions is specified as follows:

$$i\frac{\partial u}{\partial t}+\frac{1}{2}\left(\frac{\partial^2 u}{\partial x^2}+\frac{\partial^2 u}{\partial y^2}\right)+\left(|u|^2+\epsilon|v|^2\right)u=0, \tag{1.7}$$

$$i\frac{\partial v}{\partial t}+\frac{1}{2}\left(\frac{\partial^2 v}{\partial x^2}+\frac{\partial^2 v}{\partial y^2}\right)+\left(\epsilon|u|^2+|v|^2\right)v=0. \tag{1.8}$$

Initial conditions:

$$u(x,y,0)=f_1(x,y), \tag{1.9}$$

$$v(x,y,0)=f_2(x,y). \tag{1.10}$$

Boundary conditions:

$$u(x,y,t)=f_1(x,y,t), \tag{1.11}$$

$$v(x,y,t)=f_2(x,y,t). \tag{1.12}$$

Where $(x,y)\in\partial D$ and $t>0$. D is the computational domain, and the computational domain is the rectangular R^2, and ∂D is the boundary of the corresponding computational domain. The mentioned functions $f_1(x,y)$, $f_2(x,y)$, $f_1(x,y,t)$, and $f_2(x,y,t)$ are all sufficiently smooth functions. Functions u and v are known as amplitudes of two waves. Soliton waves can collide with elastic properties in a system that is integrable, but if the system in question is not elastic, the collisions may be extremely difficult to predict. These applications can be found in a wide variety of

plasma physics and nonlinear optics fields [2, 21, 75]. Such collisions for various physical arrangements have already been the subject of a great deal of research. Many diverse collision patterns, such as reflection, transmission, trapping annihilation, and mutual spiraling, are seen, but different limitations are also linked in order to maintain accuracy. Numerous studies dealing with the numerical aspect of coupled Schrödinger equations have been described in literature. Sun and Qin [62] solved the coupled $1D$ nonlinear Schrödinger problem using the multi-symplectic technique. Multi-symplectic integration was introduced by Aydin and Karasozen [8] as a solution to coupled Schrödinger equations. In that study, elastic and inelastic collision properties were numerically developed using a six-point system that was nearly identical to the multi-symplectic Preissman approach. To numerically solve the coupled nonlinear Schrödinger equation, Ismail and Taha [37] introduced the concept of a linearly implicit conservative regime. In their study, they dealt with a relevant problem using a linear implicit conservative approach. To acquire the numerical solution, Ismail [23] offered the idea of the Galerkin technique on the coupled nonlinear Schrödinger problem, where the finite element approach was used.

To numerically solve the nonlinear Schrödinger equation, Xu and Shu [72] proposed a local discontinuous Galerkin approach. Regarding N coupled nonlinear Schrödinger equations, Dehghan et al. [17] applied the meshless local Petrov-Galerkin technique, where the finite difference formula was used to estimate the first-order time derivative. A collocation strategy using radial basis functions was accustomed to approximate spatial derivatives according to Kansa's method. The concept of a split-step FD technique for the Schrödinger equation was introduced by Wang [67]. For dealing with the numerical solution of the $(2+1)D$ coupled Schrödinger equation, Zhang et al. [78] introduced the concept of symbolic computation. Via $(2+1)D$ coupled Schrödinger equations with variable coefficients, Gao et al. [19] explored the study of applications. For the purpose of obtaining a solution to the coupled Schrödinger equation, Sonnier and Christov [60] employed a conservative regime. For coupled Schrödinger equations, Sweilam and Al-Bar [64] used VIM. In that project, Ji-Huan He's Variational Iteration Method was applied. By using FDM, Ismail and Taha [26] demonstrated numerical approximation of the coupled Schrödinger problem. The alternating-direction implicit (ADI) scheme was introduced by Ismail et al. [24] to tackle the numerical solution of the $2D$ coupled Schrödinger problem. DTM was presented by Abazari & Abazari [1] to obtain a numerical solution of the coupled Schrödinger problem. Numerical analysis of solitons for the coupled Schrödinger problem was provided by Sun et al. [63]. Ismail [22] offered an explicit fourth-order method to solve the coupled Schrödinger equation, where the 4th-order central difference formula discretized the space derivative. Bashan [9] used the FD method and quartic B-spline DQM to create a mixed approach to the Schrödinger problem.

DQM is one of the most effective methods for approximating derivatives regarding a function using the linear sum of functional values at given discrete points. When compared to current methods, DQM is simple to fetch numerical solutions of PDEs. Bellman and his collaborators introduced DQM for the first time in 1972 [15]. The integral quadrature served as the first inspiration for the DQM concept. Finding weighting coefficients in DQM is the key to this procedure; therefore, the fundamental idea of the method is to do so in order to estimate the partial derivatives that are given. Numerous test functions, such as B-splines, Lagrange interpolation polynomials, Barycentric Lagrange interpolation functions, etc., can be used to obtain necessary weighting factors. Legendre polynomials and the idea of spline functions were incorporated by Bellman et al. [15] to obtain weighting coefficients. A formal formulation to determine weighting coefficients utilizing the idea of a Lagrange interpolation polynomial was then provided by Quan and Chang [52, 53].

Additionally, contributions were made by Shu and Richards [57]. One of the most crucial ideas in this field was put out by Shu [56]. Shu [55] provided an explicit formulation for quickly and easily applying weighting coefficients. To obtain weighting coefficients, Shu and Xue [58] used the Lagrange interpolation trigonometric polynomial idea. The implicit equations to determine weighting coefficients by utilizing radial basis functions were provided by Wu et al. [70]. Harmonic functions were suggested by Striz et al. [61] as a method for implicitly determining weighting coefficients.

To arrive at the Burgers-Huxley equation's numerical solution, Tomasiello (2010) [65] employed the DQM approach. Some of these techniques are presented ahead; knowledge of these techniques was gathered via researching literature. Different physics and engineering problems have been handled by various numerical techniques by developing a variety of test functions. The concept of Sinc DQM was put into practice by Korkmaz and Dag [34] to fetch solutions for

shock wave simulations numerically. To get a numerical solution of the Schrödinger equation, Bashan et al. [14] presented the perspective of a quintic B-spline-built Crank-Nicolson DQM. The weighted average DQM concept was incorporated by Jiwari et al. [28] to get a numerical approximation of Burgers' equation.

By using modified B-spline DQM, Mittal and Bhatia [45] were able to arrive at a numerical solution for the 2D hyperbolic telegraph problem. SSP-RK43 approach was applied to handle the resulting ODE system after space discretization using modified B-spline DQM. Mittal and Dahiya [48] implemented a cubic B-spline approach to deal with the 3D telegraphic equation numerically. Implementation of a cubic B-spline for space discretization produced an ODE system that was handled using a 4th-stage RK approach. Mittal and Rohila [46] employed MCB-spline DQM to achieve a numerical solution of RD system. The generated ODE was handled using the SSP-RK43 method. Arora et al. [7] approached Schrödinger issue using DQM employing a trigonometric cubic B-spline basis function. Arora and Joshi [6] used trigonometric B-spline DQM to deal with the numerical solution of Burgers' equation. Bashan et al. [12] applied MCB-spline DQM to the Schrödinger equation solution. Then, to manage the resulting set of ODEs, the SSP-RK technique was utilized. Korkmaz and Dag [32] employed the idea of the cosine expansion-based DQM to reach a numerical solution of the Schrödinger equation. Korkmaz and Dag [33] obtained a numerical solution to the advection-diffusion issue using cubic B-spline DQM. Jiwari et al. [30] used DQM to solve Dirichlet and Neumann boundary conditions for the two-dimensional hyperbolic telegraph problem. Mittal and Dahiya [49] solved the hyperbolic diffusion equation using the MCB-spline DQM technique. The obtained ODE system was handled using the SSP-RK43 technique. Korkmaz and Dag [35] used DQM to numerically solve the complex modified Korteweg-de Vries problem. Mittal and Dahiya [47] used the concept of MCB-spline-based DQM to offer numerical approximation for a class of viscous wave equations. Jiwari et al. [29] used PDQM to numerically solve a 1D hyperbolic telegraph problem. PDQM was used by Jiwari et al. [31] for the 2D Sine-Gordon equation. The notion of MCB-spline DQM was applied by Arora and Singh [5] regarding Burgers' equation. Spatial discretization was carried out using MCB-DQM, and the resultant ODE system was tackled via the SSP-RK43 method. To solve 3D wave equations, Shukla et al. [59] used an exponential MCB-spline-based DQM approach. The space discretization was performed using MCB-DQM, and the resulting system of ODE was solved using the SSP-RK54 approach.

B-splines for the modeling of free-form shapes are the most well-known basis functions in the field of CAGD. B-splines are taken into consideration for a non-decreasing knot sequence. Every B-spline basis function of degree (n) has its support interval $[t_i, t_{i+1}))$. For every half-open interval $[t_i, t_{i+1}))$, there exist $(n+1)$ non-zero B-spline basis functions. A curve defined via parameters can be originated by different polynomial segments of degree n and can be formed via a B-spline basis function with degree (n). For every segment, there is a requirement of $(n+1)$ control points. In recent years, a good amount of work has been contributed to the development of novel B-splines. Pottmann and Wagnar [50] gave the notion of the Helix spline.

GB-Splines originated from the notion of generalized tension splines along with tension parameters in [36]. Zhang [76, 77] gave the notion of CB-splines of order based upon the given space spanned by $sin(t), cos(t), t$, and 1. Wang et al. [68] studied NUAT B-spline for $k \geq 3$ in space spanned by $1, t, t^2, \cdots, t^k, cos(t), sin(t)$. Lu et al. [38] gave the idea of uniform hyperbolic polynomial B-splines for space spanned by $1, t, t^2, \cdots, t^{k-3}, cosh(t), sinh(t), (k \geq 3)$. Gang and Wang [74] introduced an extended cubic uniform B-spline and α-B spline. Fang and Wang [18] introduced the ω B-spline. Xie and Tan [71] discussed quasi-cubic B-spline via trigonometric polynomials. Cao and Wang [16] discussed non-uniform B-spline curves. Lamniia et al. [37] used tension quartic trigonometric Bezier curves with preservation of interpolation curved shapes. Wei and Wang [69] gave an idea of an orthogonal basis regarding NUAT spline space. Hajji et al. [20] implemented UAT B-spline with $4th$-order for recommendation of curves and surfaces. Gang and Wang [73] gave the notion of AHT Bezier curves and NUAHT B-spline curves. Shen and Wang [54] discussed the concept of CD B-spline. Wang et al. [68] presented NUAT B-spline spanned in space $1, t, \cdots, t^{(k-3)}, cos(t), sin(t)$, $k \geq 3$. Qian and Tang [51] presented NUAH B-spline in space $sinh(t), cosh(t), \cdots, t^n, \cdots, t, 1 (n \geq 3)$. Some of the recent advancements regarding this field are cited as [11, 41]. The results are fetched via using the MATLAB software for the numerical computation.

Differences and advantages of NUAH B-spline compared to classical B-spline.

- **Classical B-spline:** It lacks inherent adaptivity; to achieve higher accuracy, higher-degree splines or a globally refined knot sequence are required, which can increase computational cost unnecessarily in areas that do not require fine detail.
- **NUAH B-spline:** It incorporates hierarchical refinement and adaptivity, enabling localized refinement without impacting the global structure. This makes it computationally efficient and suited for problems with local irregularities or complexities.

Motivation of the study.

- **Significance of the problem:** Due to the practical relevance of coupled $1D$ and $2D$ nonlinear Schrödinger equations in areas such as quantum mechanics and nonlinear optics, this research is done.
- **Gaps in existing methods:** There are some limitations of existing numerical approaches, such as computational inefficiency, lack of stability, or challenges in handling coupled systems. That is why, via the present technique, these limitations are tried to be handled.
- **Advantages of the proposed technique:** The MCNUAH B-spline DQM for spatial discretization and the SSP-RK43 for temporal integration provide a stable, efficient, and straightforward solution. The matrix method used for stability analysis will also be elaborated upon to show the robustness of the method.

Key features of the proposed study.

Properties:

(1) Spatial discretization: This method utilizes the MCNUAH B-spline (DQM) for discretizing spatial partial derivatives, which ensures accuracy and smoothness in capturing spatial variations.
(2) Temporal integration: In this research, the SSP-RK43 (Strong Stability Preserving Runge-Kutta method of order 4 and stage 3) is employed, which is well-suited for solving stiff systems of ODEs resulting from spatial discretization.
(3) Stability analysis: Stability of the proposed scheme is investigated via a matrix method, which demonstrates the robustness of the numerical technique under given conditions.
(4) Validation: Performance is tested through four numerical experiments, and results are compared with existing literature, confirming the reliability and accuracy of the proposed method.

Characteristics:

(1) Efficiency: The scheme is efficient due to the compact nature of B-splines and the SSP-RK43 integrator, which reduces the computational cost.
(2) Simplicity: The implementation is easy to apply, which makes the approach accessible for practical applications without the requirement of complex algorithms.
(3) Accuracy: It produces highly accurate solutions that are compatible with previously published results, confirming its ability to handle $1D$ and $2D$ coupled nonlinear Schrödinger equations efficiently.

Weaknesses:

(1) Dependence on stability conditions: This method is stable under specific conditions; it might not be stable for all possible parameter sets.
(2) Sensitivity to parameter choices: The accuracy and stability of results may depend on appropriate choice of parameters such as time step size, spatial discretization resolution, and spline degree.
(3) Complexity in matrix stability analysis: While it is a robust technique, the matrix stability analysis method may add a layer of complexity, mainly for users unfamiliar with such methods.

Outline of paper: The present paper is distributed into different sections and subsections in order to make a better understanding.

- In section 2, the novel scheme NUAH B-spline DQM is developed, and formulae for the discretization of spatial partial derivatives are given.
- In subsection 2.1, a brief knowledge regarding the coupled $1D$ Schrödinger equation is provided in terms of discretizing spatial partial derivatives.
- In subsection 2.2, the formulae for discretizing spatial partial derivatives in the coupled $2D$ Schrödinger equation is mentioned.

- In subsection 2.3, the NUAH B-splines of orders 2, 3, and 4 are elaborated. The formulae regarding the improvised results are also given.
- In subsection 2.4, weighting coefficients are determined in a proper way by using the notion of the differential quadrature method. Finding the weighting coefficients in DQM is the main key, and weighting coefficients are the link between spatial partial derivatives and the functional values at different node points.
- In subsubsections 2.5.1 and 2.5.2, the implementation of the present scheme is given for the coupled $1D$ and $2D$ Schrödinger equations, respectively.
- In section 3, four numerical examples are discussed; among these four examples, the first three examples are related to the coupled $1D$ Schrödinger equation, and the fourth examples is related to the coupled $2D$ Schrödinger equation. In the same section, conserved quantities are also discussed. A comparison of the exact and numerical solutions is provided. Newly obtained results are compared with the existing results.
- In section 4, the stability of the proposed method is discussed via the matrix method.
- In section 5, the conclusion of this research work is presented. As per the knowledge of authors, NUAH B-spline-based DQM is never implemented to solve coupled $1D$ and $2D$ Schrödinger equations.

Therefore, in this work, an attempt is made to get a better numerical approximation of coupled $1D$ and $2D$ nonlinear Schrödinger equations. As in most cases, analytical solutions of such equations are not present in the literature. Therefore, this fact also increases the scope of finding the numerical approximation. In this paper, we have tried to shed light upon the elasticity property of wave amplitude also, and in this way, the elastic and inelastic interaction of solitons is identified.

2. Numerical Scheme (NUAH B-spline DQM)

2.1. Coupled $1D$ Schrödinger equation.

The $1D$-CNLSE is given as follows:

$$i\left(\frac{\partial u}{\partial t}+\delta\frac{\partial u}{\partial x}\right)+\frac{1}{2}\frac{\partial^2 u}{\partial x^2}+\left(|u|^2+\epsilon|v|^2\right)u=0,$$
$$i\left(\frac{\partial v}{\partial t}-\delta\frac{\partial v}{\partial x}\right)+\frac{1}{2}\frac{\partial^2 v}{\partial x^2}+\left(\epsilon|u|^2+|v|^2\right)v=0.$$

Initial conditions:

$$u(x,0)=f_1(x),\quad \text{and}\quad v(x,0)=f_2(x).$$

Boundary conditions:

$$\frac{\partial u}{\partial x}=0,\quad \text{and}\quad \frac{\partial v}{\partial x}=0,\quad \text{at}\quad x=x_l,\ \text{and}\ x=x_r,\ \text{for}\ t>0,$$

where the complex functions u and v can be decomposed into the real and imaginary parts and are notified as follows:

$$u(x,t)=p(x,t)+iq(x,t), \tag{2.1}$$
$$v(x,t)=r(x,t)+is(x,t). \tag{2.2}$$

The computational domain, in this case, is taken as $[a,b]$, which can be partitioned in a uniform approach with the length of each interval $h=\frac{b-a}{n}$. Where, $a=x_0<x_1<\cdots<x_n=b$. Let $\text{NUAHB}_i(x)$ be the NUAH B-spline at the knot points x_n, where $n=0,1,2,\ldots,N$. The set of NUAH B-splines can be given as $\{\text{NUAHB}_{-1},\text{NUAHB}_0,\ldots,\text{NUAHB}_{N+1}\}$.

By the differential quadrature method (DQM), the rth partial derivatives of u and v are expressed as follows:

$$u_x^{(r)}=\sum_{j=1}^{n}a_{ij}^{(r)}u(x_j), \tag{2.3}$$
$$v_x^{(r)}=\sum_{j=1}^{n}a_{ij}^{(r)}v(x_j). \tag{2.4}$$

By using $r = 1$ in the above equations, the first-order partial derivatives of u and v w.r.t. x are notified as follows:

$$u_x^{(1)} = \sum_{j=1}^{n} a_{ij}^{(1)} u(x_j), \tag{2.5}$$

$$v_x^{(1)} = \sum_{j=1}^{n} a_{ij}^{(1)} v(x_j), \tag{2.6}$$

and second-order partial derivatives of u and v w.r.t. x are notified as follows:

$$u_x^{(2)} = \sum_{j=1}^{n} a_{ij}^{(2)} u(x_j), \tag{2.7}$$

$$v_x^{(2)} = \sum_{j=1}^{n} a_{ij}^{(2)} v(x_j). \tag{2.8}$$

2.2. **Coupled $2D$ Schrödinger equation.** For the $2D$ CNLSE, the computational domain is given by $[a, b] \times [c, d]$. Let $a = x_0 < x_1 < \cdots < x_{N_1} = b$ and $c = y_0 < y_1 < \cdots < y_{N_2} = d$.

In this case, the NUAH B-splines can be denoted as $\{\text{NUAHB}_{-1}, \text{NUAHB}_0, \ldots, \text{NUAHB}_{N_1+1}\}$ and $\{\text{NUAHB}_{-1}, \text{NUAHB}_0, \ldots, \text{NUAHB}_{N_2+1}\}$ defined over $[a, b] \times [c, d]$.

By the differential quadrature method (DQM), $u(x, y, t)$ and $v(x, y, t)$ can be approximated as follows:

$$u_x = \sum_{j=1}^{N_1} a_{ij}\, u(x_j, y, t), \tag{2.9}$$

$$u_{xx} = \sum_{j=1}^{N_1} b_{ij}\, u(x_j, y, t), \tag{2.10}$$

$$u_y = \sum_{j=1}^{N_2} a'_{ij}\, u(x, y_j, t), \tag{2.11}$$

$$u_{yy} = \sum_{j=1}^{N_2} b'_{ij}\, u(x, y_j, t), \tag{2.12}$$

$$v_x = \sum_{j=1}^{N_1} a_{ij}\, v(x_j, y, t), \tag{2.13}$$

$$v_{xx} = \sum_{j=1}^{N_1} b_{ij}\, v(x_j, y, t), \tag{2.14}$$

$$v_y = \sum_{j=1}^{N_2} a'_{ij}\, v(x, y_j, t), \tag{2.15}$$

$$v_{yy} = \sum_{j=1}^{N_2} b'_{ij}\, v(x, y_j, t). \tag{2.16}$$

2.3. **NUAH B-spline:** In the same section, it is considered that NUAHB_i^k is a "non-uniform algebraic hyperbolic B-spline" of order k with given node points γ_i in a uniform distribution over $a = \gamma_1 < \gamma_2 < \gamma_3 < \cdots < \gamma_n = b$.

Therefore, a "cubic non-uniform algebraic hyperbolic B-spline" will form a basis in the domain $[a, b]$. The non-uniform algebraic hyperbolic B-spline of order two is defined as follows:

$$\mathrm{NUAH}_{i,2}(\gamma) = \begin{cases} \frac{\sinh(\gamma-\gamma_i)}{\sinh(\gamma_{i+1}-\gamma_i)}, & \gamma \in [\gamma_i, \gamma_{i+1}), \\ \frac{\sinh(\gamma_{i+2}-\gamma)}{\sinh(\gamma_{i+2}-\gamma_{i+1})}, & \gamma \in [\gamma_{i+1}, \gamma_{i+2}), \end{cases} \tag{2.17}$$

$$\mathrm{NUAH}_{i,j}(\gamma) = \int_{-\infty}^{\gamma} \left(\theta_{i,j-1}\,\mathrm{NUAH}_{i,j-1}(s)\,ds - \theta_{i+1,j-1}\,\mathrm{NUAH}_{i+1,j-1}(s)\,ds\right), \quad 3 \le j \le i, \tag{2.18}$$

and

$$\theta_{i,j} = \frac{1}{\int_{-\infty}^{\infty} \mathrm{NUAH}_{i,j}(s)\,ds}, \quad \text{where } \mathrm{NUAH}_{i,j}(s) \neq 0. \tag{2.19}$$

Via the 2^{nd} order NUAH B-spline and the provided recurrence relation, the NUAH B-spline of order three is notified as follows:

$$\mathrm{NUAH}_{i,3}(\gamma) = \int_{-\infty}^{\gamma} \left[\theta_{i,2}\,\mathrm{NUAH}_{i,2}(s)\,ds - \theta_{i+1,2}\,\mathrm{NUAH}_{i+1,2}(s)\,ds\right], \tag{2.20}$$

$$\mathrm{NUAH}_{i,3}(\gamma) = \begin{cases} \frac{\theta_{i,2}\,[\cosh(\gamma-\gamma_i)-1]}{\sinh(\gamma_{i+1}-\gamma_i)}, & \gamma \in [\gamma_i, \gamma_{i+1}), \\ 1 - \frac{\theta_{i,2}\,[\cosh(\gamma_{i+2}-\gamma)-1]}{\sinh(\gamma_{i+2}-\gamma_{i+1})} - \frac{\theta_{i+1,2}\,[\cosh(\gamma-\gamma_{i+1})-1]}{\sinh(\gamma_{i+2}-\gamma_{i+1})}, & \gamma \in [\gamma_{i+1}, \gamma_{i+2}), \\ \frac{\theta_{i+1,2}\,[\cosh(\gamma_{i+3}-\gamma)-1]}{\sinh(\gamma_{i+3}-\gamma_{i+2})}, & \gamma \in [\gamma_{i+2}, \gamma_{i+3}), \\ 0, & \text{elsewhere}, \end{cases} \tag{2.21}$$

$$\mathrm{NUAH}_{i,4}(\gamma) = \int_{-\infty}^{\gamma} \left[\theta_{i,3}\,\mathrm{NUAH}_{i,3}(s)\,ds - \theta_{i+1,3}\,\mathrm{NUAH}_{i+1,3}(s)\,ds\right], \tag{2.22}$$

$$\mathrm{NUAH}_{i,4}(\gamma) = \begin{cases} (1)\ \frac{\theta_{i-2,3}\,\theta_{i-2,2}\,[\sinh(\gamma-\gamma_{i-2})-(\gamma-\gamma_{i-2})]}{\sinh(\gamma_{i-1}-\gamma_{i-2})}, & \gamma \in [\gamma_{i-2}, \gamma_{i-1}), \\ (2)\ \theta_{i-2,3}\left[\frac{\theta_{i-2,2}[\sinh(\gamma_{i-1}-\gamma_{i-2})-(\gamma_{i-1}-\gamma_{i-2})]}{\sinh(\gamma_{i-1}-\gamma_{i-2})} + (\gamma-\gamma_{i-1})\right. & \\ \left. + \frac{\theta_{i-2,2}[\sinh(\gamma_i-\gamma)-\sinh(\gamma_i-\gamma_{i-1})+(\gamma-\gamma_{i-1})]}{\sinh(\gamma_i-\gamma_{i-1})}\right] & \\ - \frac{\theta_{i-1,2}[\sinh(\gamma-\gamma_{i-1})-(\gamma-\gamma_{i-1})]}{\sinh(\gamma_i-\gamma_{i-1})}, & \gamma \in [\gamma_{i-1}, \gamma_i), \\ (3)\ 1 - \frac{\theta_{i-2,3}\,\theta_{i-2,2}[\sinh(\gamma_{i+1}-\gamma)-(\gamma_{i+1}-\gamma)]}{\sinh(\gamma_{i+1}-\gamma_i)} & \\ -\theta_{i-1,3}\left[\frac{\theta_{i-1,2}[\sinh(\gamma_i-\gamma_{i-1})-(\gamma_i-\gamma_{i-1})]}{\sinh(\gamma_i-\gamma_{i-1})}\right. & \\ \left. + (\gamma-\gamma_i) + \frac{\theta_{i-1,2}[\sinh(\gamma_{i+1}-\gamma)-\sinh(\gamma_{i+1}-\gamma_i)+(\gamma-\gamma_i)]}{\sinh(\gamma_{i+1}-\gamma_i)}\right. & \\ \left. - \frac{\theta_{i,2}[\sinh(\gamma-\gamma_i)-(\gamma-\gamma_i)]}{\sinh(\gamma_{i+1}-\gamma_i)}\right], & \gamma \in [\gamma_i, \gamma_{i+1}), \\ (4)\ \frac{\theta_{i-1,3}\,\theta_{i,2}[\sinh(\gamma_{i+2}-\gamma)-(\gamma_{i+2}-\gamma)]}{\sinh(\gamma_{i+2}-\gamma_{i+1})}, & \gamma \in [\gamma_{i+1}, \gamma_{i+2}), \\ (5)\ 0, & \text{elsewhere}, \end{cases} \tag{2.23}$$

$$\mathrm{NUAH}'_{i,4}(\gamma)=\begin{cases}(1)\,\frac{\theta_{i-2,3}\,\theta_{i-2,2}\,[\cosh(\gamma-\gamma_{i-2})-1]}{\sinh(\gamma_{i-1}-\gamma_{i-2})}, & \gamma\in[\gamma_{i-2},\gamma_{i-1}),\\ (2)\,\theta_{i-2,3}\left[1+\frac{\theta_{i-2,2}[1-\cosh(\gamma_i-\gamma)]}{\sinh(\gamma_i-\gamma_{i-1})}-\frac{\theta_{i-1,2}[\cosh(\gamma-\gamma_{i-1})-1]}{\sinh(\gamma_i-\gamma_{i-1})}\right]\\ -\frac{\theta_{i-1,3}\,\theta_{i-1,2}[\cosh(\gamma-\gamma_{i-1})-1]}{\sinh(\gamma_i-\gamma_{i-1})}, & \gamma\in[\gamma_{i-1},\gamma_i),\\ (3)\,-\frac{\theta_{i-2,3}\,\theta_{i-1,2}[1-\cosh(\gamma_{i+1}-\gamma)]}{\sinh(\gamma_{i+1}-\gamma_i)}\\ -\theta_{i+1,3}\left[1+\frac{\theta_{i-1,2}[1-\cosh(\gamma_{i+1}-\gamma)]}{\sinh(\gamma_{i+1}-\gamma_i)}-\frac{\theta_{i,2}[\cosh(\gamma-\gamma_i)-1]}{\sinh(\gamma_{i+1}-\gamma_i)}\right], & \gamma\in[\gamma_i,\gamma_{i+1}),\\ (4)\,\frac{\theta_{i-1,3}\,\theta_{i,2}[1-\cosh(\gamma_{i+2}-\gamma)]}{\sinh(\gamma_{i+2}-\gamma_{i+1})}, & \gamma\in[\gamma_{i+1},\gamma_{i+2}),\\ (5)\,0, & \text{elsewhere,}\end{cases}\tag{2.24}$$

$$\mathrm{NUAH}''_{i,4}(x)=\begin{cases}(1)\,\frac{\theta_{i-2,3}\,\theta_{i-2,2}\,\sinh(x-x_{i-2})}{\sinh(x_{i-1}-x_{i-2})}, & x\in[x_{i-2},x_{i-1}),\\ (2)\,\theta_{i-2,3}\left[\frac{\theta_{i-2,2}\sinh(x_i-x)}{\sinh(x_i-x_{i-1})}-\frac{\theta_{i-1,2}\sinh(x-x_{i-1})}{\sinh(x_i-x_{i-1})}\right]\\ -\frac{\theta_{i-1,3}\,\theta_{i-1,2}[\cosh(x-x_{i-1})-1]}{\sinh(x_i-x_{i-1})}, & x\in[x_{i-1},x_i),\\ (3)\,-\frac{\theta_{i-2,3}\,\theta_{i-1,2}\sinh(x_{i+1}-x)}{\sinh(x_{i+1}-x_i)}\\ -\theta_{i+1,3}\left[\frac{\theta_{i-1,2}\sinh(x_{i+1}-x)}{\sinh(x_{i+1}-x_i)}-\frac{\theta_{i,2}\sinh(x-x_i)}{\sinh(x_{i+1}-x_i)}\right], & x\in[x_i,x_{i+1}),\\ (4)\,\frac{\theta_{i-1,3}\,\theta_{i,2}\sinh(x_{i+2}-x)}{\sinh(x_{i+2}-x_{i+1})}, & x\in[x_{i+1},x_{i+2}),\\ (5)\,0, & \text{elsewhere.}\end{cases}\tag{2.25}$$

TABLE 1. NUAH B-spline and derivatives.

	γ_{i-2}	γ_{i-1}	γ_i	γ_{i+1}	γ_{i+2}
$\mathrm{NUAH}_{i,4}(\gamma_i)$	0	A	B	C	0
$\mathrm{NUAH}'_{i,4}(\gamma_i)$	0	D	0	F	0
$\mathrm{NUAH}''_{i,4}(\gamma_i)$	0	G	H	I	0

Calculated values:

$$A=\frac{\theta_{i-2,3}\,\theta_{i-2,2}\,[\sinh(h)-h]}{\sinh(h)},$$

$$B=1-\frac{\theta_{i-2,3}\,\theta_{i-2,2}\,[\sinh(h)-h]}{\sinh(h)}-\frac{\theta_{i-1,3}\,\theta_{i-1,2}\,[\sinh(h)-h]}{\sinh(h)},$$

$$C=\frac{\theta_{i-1,3}\,\theta_{i,2}\,[\sinh(h)-h]}{\sinh(h)},\quad D=\frac{1}{2h},\quad F=-\frac{1}{2h},$$

$$G=\theta_{i-2,3}\,\theta_{i-2,2},\quad H=-\theta_{i-2,3}\,\theta_{i-1,2}-\theta_{i+1,3}\,\theta_{i-1,2},\quad I=\delta_{i-1,3}\,\delta_{i,2},$$

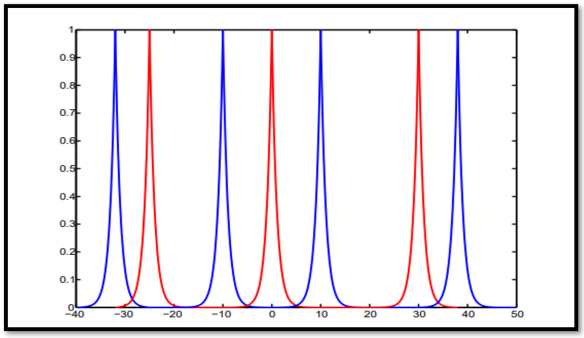

FIGURE 2. The NUAH B-spline of order 2.

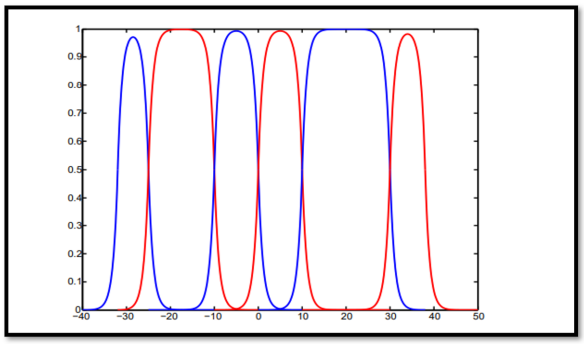

FIGURE 3. The NUAH B-spline of order 3.

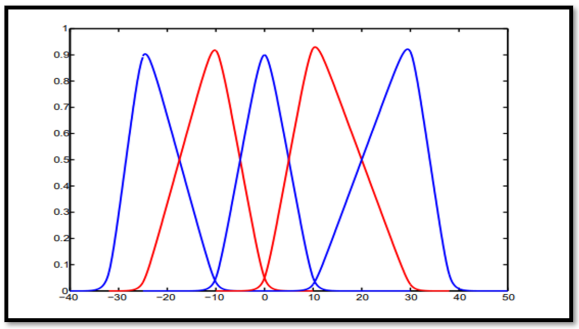

FIGURE 4. The NUAH B-spline of order 4.

$$\theta_{i-2,2} = \frac{\sinh(h)}{2[\cosh(h)-1]}, \quad \theta_{i-1,2} = \frac{\sinh(h)}{2[\cosh(h)-1]}, \quad \theta_{i-1,3} = \frac{1}{h}, \quad \theta_{i-2,3} = \frac{1}{h}.$$

Where $\{\text{NUAHB}_0(x), \text{NUAHB}_1(x), \ldots, \text{NUAHB}_N(x), \text{NUAHB}_{N+1}(x)\}$ forms a basis in the specified domain. Figures 2-4, show graphs for the NUAH B-spline.

Eq. (2.23) and Table 1 can be used to create a modified cubic non-uniform algebraic hyperbolic B-spline in such a way that the resulting matrix system becomes diagonally dominant [5] to enhance the results.

It is possible to generate improved values using the following set of equations:

$$\begin{aligned}
\mathrm{MNUAH}_1(x) &= \mathrm{NUAHB}_1(x) + 2\,\mathrm{NUAHB}_0(x),\\
\mathrm{MNUAH}_2(x) &= \mathrm{NUAHB}_2(x) - \mathrm{NUAHB}_0(x),\\
\mathrm{MNUAH}_j(x) &= \mathrm{NUAHB}_j(x), \quad (j = 3,4,5,\ldots,N-2),\\
\mathrm{MNUAH}_{N-1}(x) &= \mathrm{NUAHB}_{N-1}(x) - \mathrm{NUAHB}_{N+1}(x),\\
\mathrm{MNUAH}_N(x) &= \mathrm{NUAHB}_N(x) + 2\,\mathrm{NUAHB}_{N+1}(x).
\end{aligned}$$

2.4. **Determination of weighting coefficients:** We may approximate the first-order derivative as follows:

$$\mathrm{MNUAH}_k^{(1)}(x_i) = \sum_{j=1}^{n} a_{ij}^{(1)}\,\mathrm{MNUAH}_k(x_j). \tag{2.26}$$

At x_1: The following set of equations are obtained by applying formulas in Eqs. (2.23), (2.24), and (2.25) with Table 1 to Eq. (2.26) for various values of k:

$$\begin{aligned}
k=1: &\quad \mathrm{MNUAH}_1'(x_1) = \sum_{j=1}^{n} a_{1j}^{(1)}\,\mathrm{MNUAH}_1(x_j) = a_{11}^{(1)}[B+2C] + a_{12}^{(1)}[C],\\
k=2: &\quad \mathrm{MNUAH}_2'(x_1) = \sum_{j=1}^{n} a_{1j}^{(1)}\,\mathrm{MNUAH}_2(x_j) = a_{11}^{(1)}[A-C] + a_{12}^{(1)}[B] + a_{13}^{(1)}[C],\\
k=3: &\quad \mathrm{MNUAH}_3'(x_1) = \sum_{j=1}^{n} a_{1j}^{(1)}\,\mathrm{MNUAH}_3(x_j) = a_{12}^{(1)}[A] + a_{13}^{(1)}[B] + a_{14}^{(1)}[C],\\
&\quad\ \vdots\\
k=n: &\quad \mathrm{MNUAH}_n'(x_1) = \sum_{j=1}^{n} a_{1j}^{(1)}\,\mathrm{MNUAH}_n(x_j) = a_{1,n-1}^{(1)}[A] + a_{1n}^{(1)}[B+2A].
\end{aligned}$$

Using the above set of equations at x_1 for $k = 1,2,3,\ldots,n$, we will obtain the following tridiagonal system of algebraic equations:

$$A\,\vec{a}^{(1)}[i] = \vec{V}[i], \quad \text{where} \quad i = 1,2,3,\ldots,n,$$

$$A = \begin{bmatrix}
B+2C & A-C & & & & \\
C & B & A & & & \\
 & C & B & A & & \\
\vdots & \vdots & \ddots & \ddots & \vdots & \\
 & & A & B & C-A & \\
 & & & C & B+2A
\end{bmatrix}, \qquad \vec{a}^{(1)}[1] = \begin{bmatrix} a_{1,1}^{(1)} \\ a_{1,2}^{(1)} \\ a_{1,3}^{(1)} \\ \vdots \\ a_{1,N-1}^{(1)} \\ a_{1,N}^{(1)} \end{bmatrix},$$

$$\vec{V}[1] = \begin{bmatrix} \mathrm{MNUAH}_1'(x_1) \\ \mathrm{MNUAH}_2'(x_1) \\ \mathrm{MNUAH}_3'(x_1) \\ \vdots \\ \mathrm{MNUAH}_{n-1}'(x_1) \\ \mathrm{MNUAH}_n'(x_1) \end{bmatrix} = \begin{bmatrix} 2F \\ D-F \\ 0 \\ \vdots \\ 0 \end{bmatrix}.$$

At grid point x_2: The following set of equations is obtained by applying formulas in Eqs. (2.23), (2.24), and (2.25) with Table 1 to Eq. (2.26) for various values of k:

$$\vec{a}^{(1)}[2] = \begin{bmatrix} a_{21}^{(1)} \\ a_{22}^{(1)} \\ a_{23}^{(1)} \\ \vdots \\ a_{2,N-1}^{(1)} \\ a_{2,N}^{(1)} \end{bmatrix}, \quad \vec{V}[2] = \begin{bmatrix} \text{MNUAH}_1'(x_2) \\ \text{MNUAH}_2'(x_2) \\ \text{MNUAH}_3'(x_2) \\ \vdots \\ \text{MNUAH}_{n-1}'(x_2) \\ \text{MNUAH}_n'(x_2) \end{bmatrix} = \begin{bmatrix} F \\ 0 \\ D \\ 0 \\ \vdots \\ 0 \end{bmatrix},$$

$$\vdots$$

At grid point x_n: The following set of equations is obtained by applying formulas in Eqs. (2.23), (2.24), and (2.25) with Table 1 to Eq. (2.26) for various values of k:

$$\vec{a}^{(1)}[n] = \begin{bmatrix} a_{n,1}^{(1)} \\ a_{n,2}^{(1)} \\ a_{n,3}^{(1)} \\ \vdots \\ a_{n,n-1}^{(1)} \\ a_{n,n}^{(1)} \end{bmatrix}, \quad \vec{V}[n] = \begin{bmatrix} \text{MNUAH}_1'(x_n) \\ \text{MNUAH}_2'(x_n) \\ \text{MNUAH}_3'(x_n) \\ \vdots \\ \text{MNUAH}_{n-1}'(x_n) \\ \text{MNUAH}_n'(x_n) \end{bmatrix} = \begin{bmatrix} 0 \\ 0 \\ \vdots \\ 0 \\ F-D \\ 2D \end{bmatrix}.$$

Similarly, to find weighting coefficients of order n where $n \geq 2$, it is notified as follows from [55]

$$a_{ij}^{(r)} = r\left[a_{ij}^{(1)} a_{ii}^{(r-1)} - \frac{a_{ij}^{(r-1)}}{x_i - x_j}\right], \quad \text{for } i \neq j, \tag{2.27}$$

$$a_{ii}^{(r)} = -\sum_{\substack{j=1 \\ j\neq i}}^{N} a_{ij}^{(r)}, \quad \text{for } i = j, \tag{2.28}$$

$$b_{ij}^{(r)} = r\left[b_{ij}^{(1)} b_{ii}^{(r-1)} - \frac{b_{ij}^{(r-1)}}{y_i - y_j}\right], \quad \text{for } i \neq j, \tag{2.29}$$

$$b_{ii}^{(r)} = -\sum_{\substack{j=1 \\ j\neq i}}^{N} b_{ij}^{(r)}, \quad \text{for } i = j. \tag{2.30}$$

2.5. **Implementation of scheme.**

2.5.1. *Upon 1D CNLS equation.* Upon the implementing the DQM approximation in $1D$ CNLSE, the following equations are given:

$$\frac{\partial u}{\partial t} = -\delta \sum_{j=1}^{n} a_{ij}^{(1)} u(x_j) + \frac{i}{2} \sum_{j=1}^{n} a_{ij}^{(2)} u(x_j) + i\left[|u|^2 + \epsilon|v|^2\right] u, \tag{2.31}$$

$$\frac{\partial v}{\partial t} = \delta \sum_{j=1}^{n} a_{ij}^{(1)} v(x_j) + \frac{i}{2} \sum_{j=1}^{n} a_{ij}^{(2)} v(x_j) + i\left[\epsilon|u|^2 + |v|^2\right] v. \tag{2.32}$$

2.5.2. *Upon the 2D CNLS equation.* By using the formulae of DQM approximation in the $2D$ CNLS equation, the following equations will be obtained:

$$\frac{\partial u}{\partial t} = \frac{i}{2}\left[\sum_{j=1}^{N_1} b_{ij}\, u(x_j, y, t) + \sum_{j=1}^{N_2} b'_{ij}\, u(x, y_j, t)\right] + i\left[|u|^2 + \epsilon|v|^2\right] u, \tag{2.33}$$

$$\frac{\partial v}{\partial t} = \frac{i}{2}\left[\sum_{j=1}^{N_1} b_{ij}\, v(x_j, y, t) + \sum_{j=1}^{N_2} b'_{ij}\, v(x, y_j, t)\right] + i\left[\epsilon|u|^2 + |v|^2\right] v. \tag{2.34}$$

The conserved quantities here are calculated with the aid of the trapezoidal rule, and L_∞ errors are obtained with the following formulae:

$$L_\infty u = \max\left[\|u\| - (\|p^{\text{num}}\| + i\|q^{\text{num}}\|)\right], \tag{2.35}$$

$$L_\infty v = \max\left[\|v\| - (\|r^{\text{num}}\| + i\|s^{\text{num}}\|)\right]. \tag{2.36}$$

3. Numerical Examples

The effectiveness and precision of the current scheme have been discussed in this section using four numerical experiments, the first three of which are related to the idea of coupled $1D$ Schrödinger equations and the fourth of which is related to coupled $2D$ Schrödinger equations. Obtained results are contrasted with previous findings. It is also explained how elastic and inelastic interactions between solitons can be used to determine if a given interaction has an elastic quality or not.

Example 3.1. Single soliton: Considered $1D$ CNLS Eqs. (1.1) and (1.2) with the following initial conditions:

$$u(x,0) = \sqrt{\frac{2\alpha}{1+\epsilon}}\,\operatorname{sech}\left(\sqrt{2\alpha}\,x\right)\exp\left[i\,(\nu-\delta)x\right], \tag{3.1}$$

$$v(x,0) = \sqrt{\frac{2\alpha}{1+\epsilon}}\,\operatorname{sech}\left(\sqrt{2\alpha}\,x\right)\exp\left[i\,(\nu+\delta)x\right], \tag{3.2}$$

where e and α are constant values. Boundary conditions imposed are natural boundary conditions:

$$\frac{\partial u}{\partial x} = 0, \quad \text{when } x = x_l, x_r,\ t > 0, \tag{3.3}$$

$$\frac{\partial v}{\partial x} = 0, \quad \text{when } x = x_l, x_r,\ t > 0. \tag{3.4}$$

In Table 2, L_∞ errors for the first wave amplitude are obtained at different values of t and $\Delta t = 0.01, 0.003$, and 0.007, respectively, for $\delta = 0.5$ and $\epsilon = 1$.

In Table 3, the L_∞ error norm for the second wave amplitude is provided at different values of t and for $\Delta t = 0.01, 0.003$, and 0.007, respectively, for $\delta = 0.5$ and $\epsilon = 1$.

In Table 4, the first and second conserved quantities are shown at time levels $t = 5, 10, 15, 20$, and 25, respectively, for $\delta = 0.5$ and $\epsilon = 1$.

In Table 5, conserved quantities are compared with [26] at time levels $t = 10, 20, 30, 40$, and 50 for $\delta = 0.5$ and $\epsilon = \frac{2}{3}$, which shows that the obtained quantities I_1 and I_2 are almost conserved.

In Table 6, the L_∞ error norm for the first wave amplitude is given at time levels $t = 4, 8, 12, 16$, and 20 for $\Delta t = 0.1, 0.08$, and 0.04, respectively, for $\epsilon = \frac{2}{3}$ and $\delta = 0.5$.

In Figures 5 and 6, graphical matching solutions of u and v components are shown at time levels $t = 5, 10, 15$, and 20, respectively, for $\delta = 0.5$ and $\epsilon = \frac{2}{3}$. A good agreement is found between the exact and numerical solutions for u and v components.

TABLE 2. L_∞ errors of u for $h = 0.2$, $N = 501$, $\delta = 0.5$, $\alpha = 1$, $\nu = 1$, and $\epsilon = 1$, for different values of Δt regarding Example 3.1.

t	$\Delta t = 0.01$	$\Delta t = 0.003$	$\Delta t = 0.007$
2	8.3595×10^{-7}	2.2550×10^{-8}	2.8603×10^{-7}
4	1.6723×10^{-6}	4.5144×10^{-8}	5.7320×10^{-7}
6	2.5081×10^{-6}	6.7724×10^{-8}	8.6019×10^{-7}
8	3.3442×10^{-6}	9.0276×10^{-8}	1.1462×10^{-6}
10	4.1804×10^{-6}	1.1287×10^{-7}	1.4334×10^{-6}

TABLE 3. L_∞ errors of v for $h = 0.2$, $N = 501$, $\delta = 0.5$, $\alpha = 1$, $\nu = 1$, and $\epsilon = 1$, for different values of Δt regarding Example 3.1.

t	$\Delta t = 0.01$	$\Delta t = 0.003$	$\Delta t = 0.007$
2	8.3594×10^{-7}	2.2550×10^{-8}	2.8602×10^{-7}
4	1.6723×10^{-6}	4.5147×10^{-8}	5.7321×10^{-7}
6	2.5082×10^{-6}	6.7728×10^{-8}	8.6020×10^{-7}
8	3.3442×10^{-6}	9.0282×10^{-8}	1.1463×10^{-6}
10	4.1805×10^{-6}	1.1287×10^{-7}	1.4334×10^{-6}

TABLE 4. Presentation of conserved quantities for $h = 0.2$, $N = 501$, $\delta = 0.5$, $\alpha = 1$, $\nu = 1$, $\epsilon = 1$, and $\Delta t = 0.01$ regarding Example 3.1.

t	First conserved quantity I_1	Second conserved quantity I_2
5	1.414211	1.414211
10	1.414209	1.414209
15	1.414206	1.414206
20	1.414204	1.414204
25	1.414202	1.414202

TABLE 5. Comparison of conserved quantities where $N = 501$, $\Delta t = 0.01$, $\nu = 1.0$, $\delta = 0.5$, $\alpha = 1.0$, and $\epsilon = \frac{2}{3}$ regarding Example 3.1.

t	Conserved quantity [26]	I_1 [Present]	I_2 [Present]
10	1.302711	1.697050	1.697050
20	1.302713	1.697045	1.697045
30	1.302706	1.697040	1.697040
40	1.302691	1.697034	1.697034
50	1.302688	1.697029	1.697029

Example 3.2. Collision of two solitons: In this example, $1D$ coupled CNLS Eqs. (1.1) and (1.2) are given with the following initial conditions:

$$u(x,0) = \sum_{j=1}^{2} \left[\sqrt{\frac{2\alpha_j}{1+\epsilon}} \operatorname{sech}\left(\sqrt{2\alpha_j}\, x_j\right) \exp\left(i\left(\nu_j - \delta\right)x_j\right) \right], \tag{3.5}$$

$$v(x,0) = \sum_{j=1}^{2} \left[\sqrt{\frac{2\alpha_j}{1+\epsilon}} \operatorname{sech}\left(\sqrt{2\alpha_j}\, x_j\right) \exp\left(i\left(\nu_j + \delta\right)x_j\right) \right], \tag{3.6}$$

TABLE 6. Comparison of L_∞ errors for the first wave amplitude where $N = 201$, $e = \frac{2}{3}$, $\alpha = 1$, $[-20, 80]$, $\delta = 0.5$, $\nu = 1$ at different time levels and Δt regarding Example 3.1.

t	$\Delta t = 0.1$		$\Delta t = 0.08$		$\Delta t = 0.04$	
	L_∞ ([26])	L_∞ (Present)	L_∞ ([26])	L_∞ (Present)	L_∞ ([26])	L_∞ (Present)
4	0.0151	1.5612×10^{-3}	0.0145	8.2503×10^{-4}	0.0026	1.0782×10^{-4}
8	0.0288	3.2978×10^{-3}	0.0278	1.6982×10^{-3}	0.0037	4.7288×10^{-5}
12	0.0422	5.1807×10^{-3}	0.0403	2.6276×10^{-3}	0.0028	-1.6355×10^{-4}
16	0.0557	7.2194×10^{-3}	0.0533	3.7363×10^{-3}	0.0036	-2.8901×10^{-4}
20	0.0693	9.3457×10^{-3}	0.0664	5.0003×10^{-3}	0.0050	-3.5753×10^{-4}

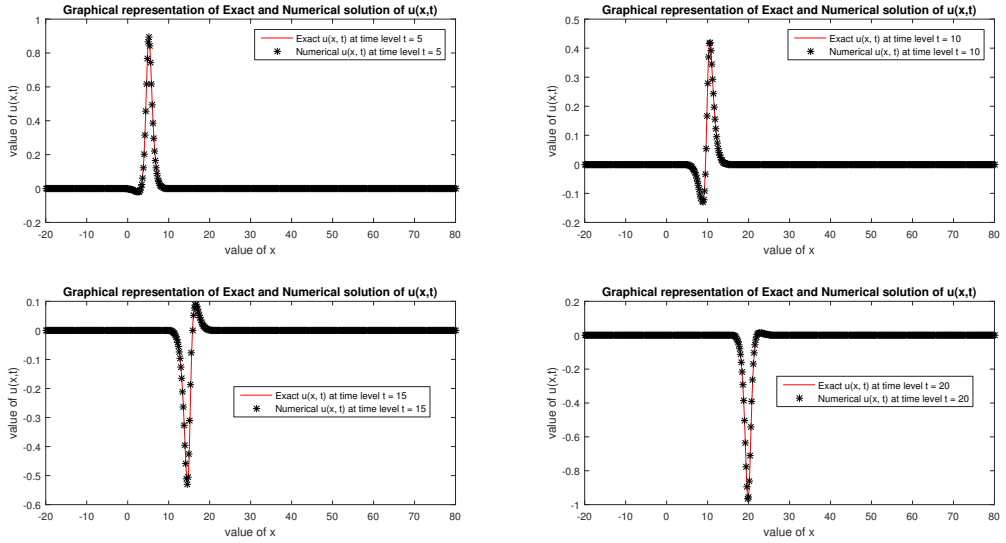

FIGURE 5. Graphical representation of solutions for first wave amplitude at $N = 501$, $\Delta t = 0.0$, $\delta = 0.5$, $\alpha = 1$, $\nu = 1$, and $e = \frac{2}{3}$ regarding Example 3.1.

which can be expressed as follows:

$$u(x,0) = \sqrt{\frac{2\alpha_1}{1+\epsilon}}\,\mathrm{sech}\left(\sqrt{2\alpha_1}\,x_1\right)\exp\left(i\,(\nu_1-\delta)x_1\right) + \sqrt{\frac{2\alpha_2}{1+\epsilon}}\,\mathrm{sech}\left(\sqrt{2\alpha_2}\,x_2\right)\exp\left(i\,(\nu_2-\delta)x_2\right), \tag{3.7}$$

$$v(x,0) = \sqrt{\frac{2\alpha_1}{1+\epsilon}}\,\mathrm{sech}\left(\sqrt{2\alpha_1}\,x_1\right)\exp\left(i\,(\nu_1+\delta)x_1\right) + \sqrt{\frac{2\alpha_2}{1+\epsilon}}\,\mathrm{sech}\left(\sqrt{2\alpha_2}\,x_2\right)\exp\left(i\,(\nu_2+\delta)x_2\right), \tag{3.8}$$

where $\nu_1 > \nu_2$. Boundary conditions imposed are natural, i.e.,

$$\frac{\partial u}{\partial x} = 0 \quad \text{at } x = x_l, x_r \text{ and } t > 0, \tag{3.9}$$

$$\frac{\partial v}{\partial x} = 0 \quad \text{at } x = x_l, x_r \text{ and } t > 0. \tag{3.10}$$

In this example, elaboration is given for the interaction of solitons. In Table 7, conserved quantities I_1 and I_2 are shown at different values of t and for different δ and e. It is observed that both identities are almost conserved on changing the time levels. In Table 8, conserved quantities are discussed at different values of t for $\delta = 0.2$, $e = 1$ and $\delta = 0.5$, e =1. In Table 9, the first conserved quantity is compared with [26] at $t = 10$, 20, 30, 40, and 50 for $\delta = 0.2$ and $\delta = 0.5$, respectively. In Table 10, L_∞ error norms of first and second wave amplitudes are discussed at $t = 10$, 20, 30, 40, and 50. In Figures 7 and 8, exact and numerical approximations are matched at different time

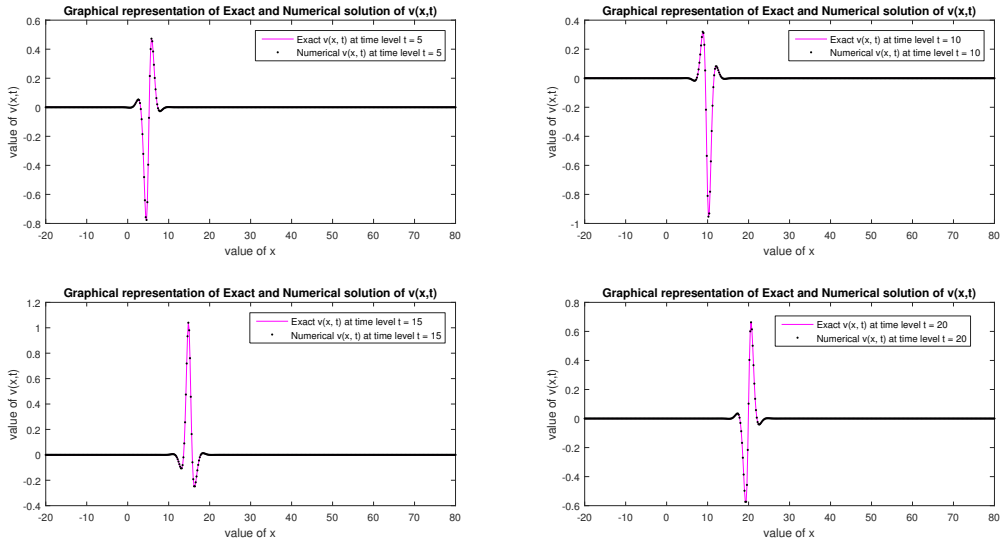

FIGURE 6. Graphical representation of solutions for second wave amplitude at $N = 501$, $\Delta t = 0.0$, $\delta = 0.5$, $\alpha = 1$, $\nu = 1$, and $e = \frac{2}{3}$ regarding Example 3.1.

levels for first and second wave amplitudes, respectively. From Figures 9-16, the elastic behavior of the interaction is shown with the changed time levels. It has been observed that for the different values of δ and e, the interaction of two solitons is inelastic/partially inelastic.

TABLE 7. Conserved quantities for parameters $N = 501$, $\Delta t = 0.01$, $\alpha_1 = 1$, $\alpha_2 = 0.5$, $\nu_1 = 1$, and $\nu_2 = 0.1$ for different δ and ϵ, $x_l = -20$, and $x_r = 80$ regarding Example 3.2.

t	I_1 $(\delta = 0.2, \epsilon = \frac{2}{3})$	I_2 $(\delta = 0.2, \epsilon = \frac{2}{3})$	I_1 $(\delta = 0.5, \epsilon = \frac{2}{3})$	I_2 $(\delta = 0.5, \epsilon = \frac{2}{3})$
5	2.89705	2.89705	2.89705	2.89705
10	2.89705	2.89705	2.89705	2.89705
15	2.89704	2.89704	2.89704	2.89704
20	2.89704	2.89704	2.89704	2.89704
25	2.89704	2.89704	2.89704	2.89704

TABLE 8. Conserved quantities for parameters $N = 501$, $\Delta t = 0.01$, $\alpha_1 = 1$, $\alpha_2 = 0.5$, $\nu_1 = 1$, and $\nu_2 = 0.1$ for different δ and ϵ, $x_l = -20$, and $x_r = 80$ regarding Example 3.2.

t	I_1 $(\delta = 0.2, \epsilon = 1)$	I_2 $(\delta = 0.2, \epsilon = 1)$	I_1 $(\delta = 0.5, \epsilon = 1)$	I_2 $(\delta = 0.5, \epsilon = 1)$
5	2.41421	2.41421	2.41421	2.41421
10	2.41420	2.41420	2.41420	2.41420
15	2.41420	2.41420	2.41420	2.41420
20	2.41420	2.41420	2.41420	2.41420
25	2.41420	2.41420	2.41420	2.41420

TABLE 9. Comparison of conserved quantities for parameters $N = 201$, $\Delta t = 0.01$, $\alpha_1 = 1$, $\alpha_2 = 0.5$, $\nu_1 = 1$, $\nu_2 = 0.1$ for different δ and ϵ, $x_l = -20$, and $x_r = 80$ regarding Example 3.2.

t	$\delta = 0.2$		$\delta = 0.5$	
	I_1 ([26])	I_1 (Present)	I_1 ([26])	I_1 (Present)
10	1.702074	1.60969	1.702074	1.60995
20	1.702074	1.61012	1.702074	1.61087
30	1.702073	1.61045	1.702073	1.61171
40	1.702064	1.61080	1.702972	1.61325
50	1.701613	1.61150	1.702070	1.61874

TABLE 10. L_∞ error for two soliton interaction for parameters $N = 201$, $\alpha_1 = 1$, $\alpha_2 = 0.5$, $\nu_1 = 1$, $\nu_2 = 0.1$, $\epsilon = \frac{2}{3}$, for different Δt at different time levels, $x_l = -20$, and $x_r = 80$ regarding Example 3.2.

t	$\Delta t = 0.01$		$\Delta t = 0.03$		$\Delta t = 0.05$	
	$L_\infty u$	$L_\infty v$	$L_\infty u$	$L_\infty v$	$L_\infty u$	$L_\infty v$
10	-3.2358×10^{-4}	2.7128×10^{-4}	-2.0447×10^{-4}	3.7432×10^{-4}	2.2409×10^{-4}	7.5496×10^{-4}
20	-3.0674×10^{-3}	-1.1401×10^{-3}	-2.7398×10^{-3}	-8.8920×10^{-4}	-1.6068×10^{-3}	5.9576×10^{-6}
30	-2.7832×10^{-1}	-3.1386×10^{-1}	-2.7734×10^{-1}	-3.1308×10^{-1}	-2.7402×10^{-1}	-3.1031×10^{-1}
40	-2.8149×10^{-3}	2.3391×10^{-3}	-1.2439×10^{-3}	3.4603×10^{-3}	3.7715×10^{-3}	7.3799×10^{-3}
50	-7.2414×10^{-3}	5.3935×10^{-3}	-5.0445×10^{-3}	6.7928×10^{-3}	1.7305×10^{-3}	1.1511×10^{-2}

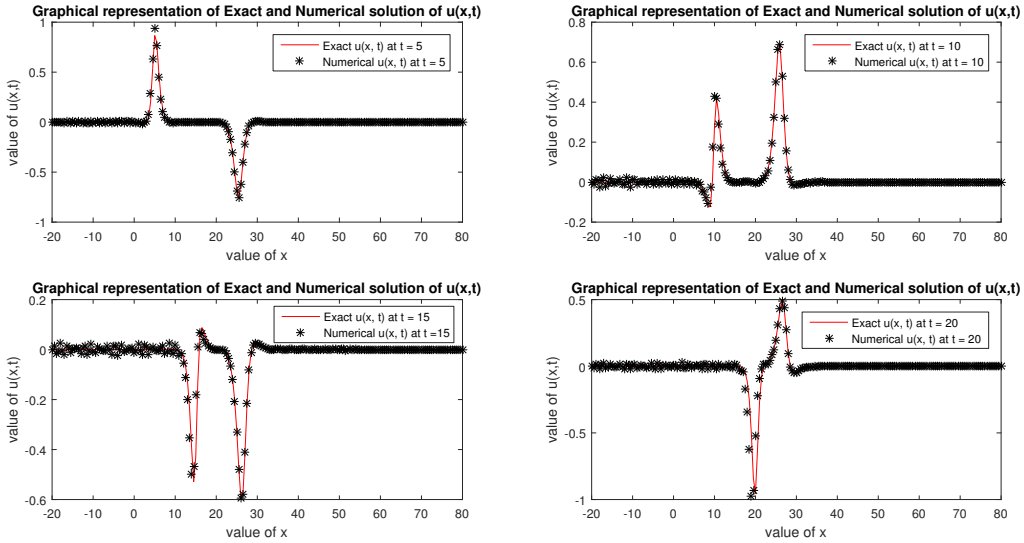

FIGURE 7. Graphical matching of exact and numerical $u(x,t)$ for $N = 201$, $\Delta t = 0.05$, $\delta = 0.5$, $\alpha_1 = 1$, $\alpha_2 = 0.5$, $\nu_1 = 1$, $\nu_2 = 0.1$, and $e = 2/3$ at time levels 5, 10, 15, and 20, respectively, regarding Example 3.2.

Example 3.3. Collision of three solitons: Considered $1D$ coupled CNLS Eqs. (1.1) and (1.2) as follows:
Initial conditions:

$$u(x,0) = \sum_{j=1}^{3} f_j(x), \tag{3.11}$$

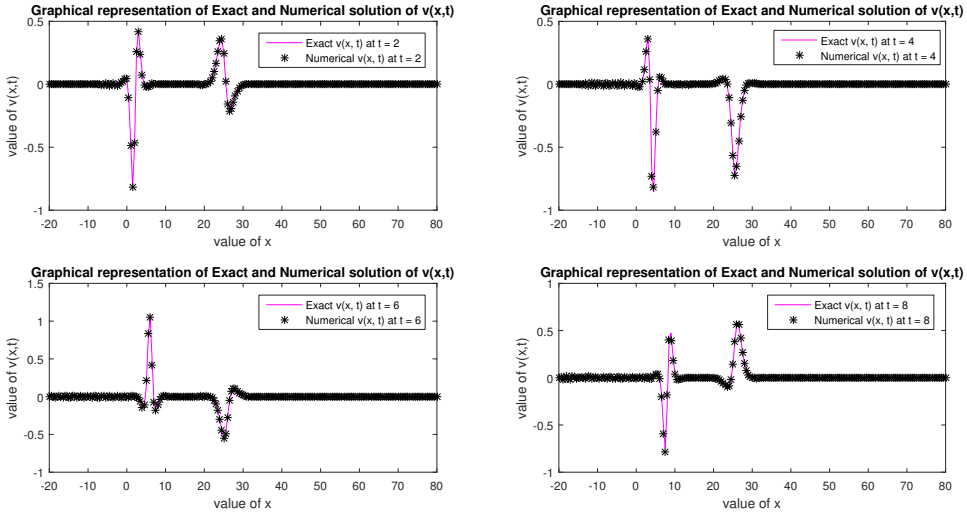

FIGURE 8. Graphical matching of exact and numerical $v(x,t)$ for $N = 201$, $\Delta t = 0.05$, $\delta = 0.5$, $\alpha_1 = 1$, $\alpha_2 = 0.5$, $\nu_1 = 1$, $\nu_2 = 0.1$, $e = 2/3$ at time levels 2, 4, 6, and 8, respectively, regarding Example 3.2.

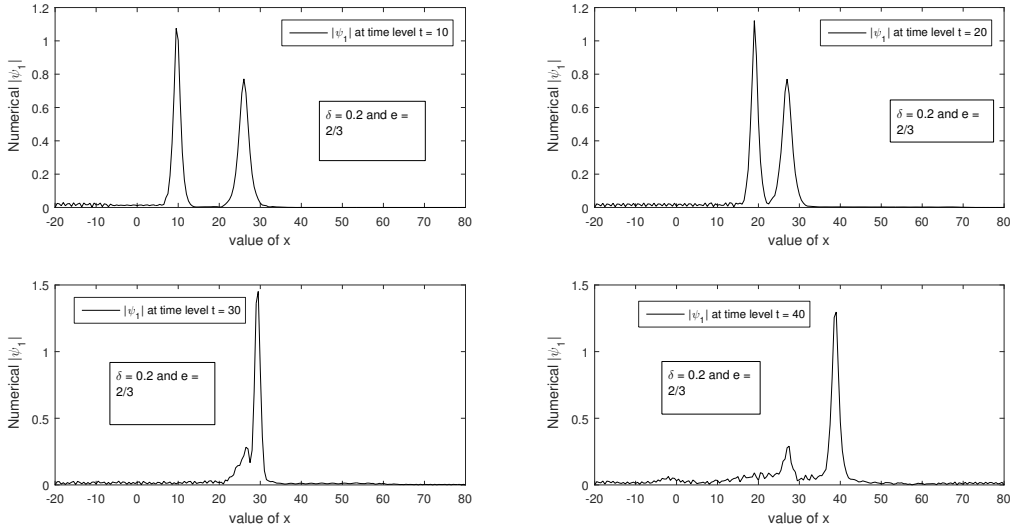

FIGURE 9. The numerical value of $|\Psi_1|$ or $|u|$ for $N = 201$, $\delta = 0.2$, $e = 2/3$, $\alpha_1 = 1$, $\alpha_2 = 0.5$, $\nu_1 = 1$, $\nu_2 = 0.1$, $\Delta t = 0.05$ at $t = 10$, 20, 30, and 40, respectively, regarding Example 3.2.

$$f_j(x) = \sqrt{\frac{2\alpha_j}{1+\epsilon}}\,\mathrm{sech}\left(\sqrt{2\alpha_j}\,x_j\right)\exp\left(i\,(\nu_j - \delta)x_j\right),$$
$$v(x,0) = \sum_{k=1}^{3} f_k(x), \tag{3.12}$$

$$f_k(x) = \sqrt{\frac{2\alpha_k}{1+\epsilon}}\,\mathrm{sech}\left(\sqrt{2\alpha_k}\,x_k\right)\exp\left(i\left(\nu_k+\delta\right)x_k\right).$$

In simpler form, initial conditions are specified as follows:

$$\begin{aligned} u(x,0) = &\sqrt{\frac{2\alpha_1}{1+\epsilon}}\,\mathrm{sech}\left(\sqrt{2\alpha_1}\,x_1\right)\exp\left(i(\nu_1-\delta)x_1\right) + \sqrt{\frac{2\alpha_2}{1+\epsilon}}\,\mathrm{sech}\left(\sqrt{2\alpha_2}\,x_2\right)\exp\left(i(\nu_2-\delta)x_2\right) \\ &+ \sqrt{\frac{2\alpha_3}{1+\epsilon}}\,\mathrm{sech}\left(\sqrt{2\alpha_3}\,x_3\right)\exp\left(i(\nu_3-\delta)x_3\right), \end{aligned} \tag{3.13}$$

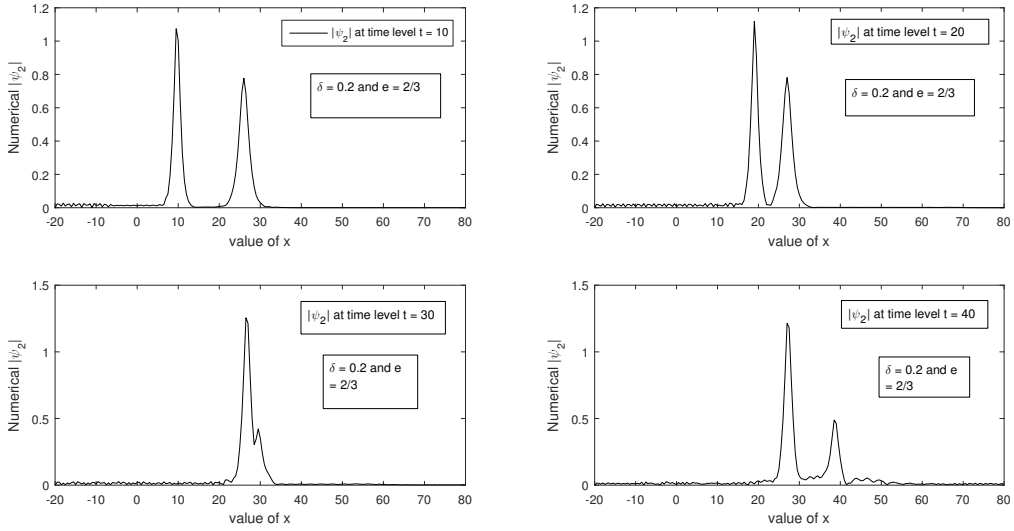

FIGURE 10. The numerical value of $|\Psi_2|$ or $|v|$ for $N = 201$, δ= 0.2, $e = 2/3$, $\alpha_1 = 1$, $\alpha_2 = 0.5$, $\nu_1 = 1$, $\nu_2 = 0.1$, and $\Delta t = 0.05$ at $t = 10$, 20, 30, and 40, respectively,, regarding Example 3.2.

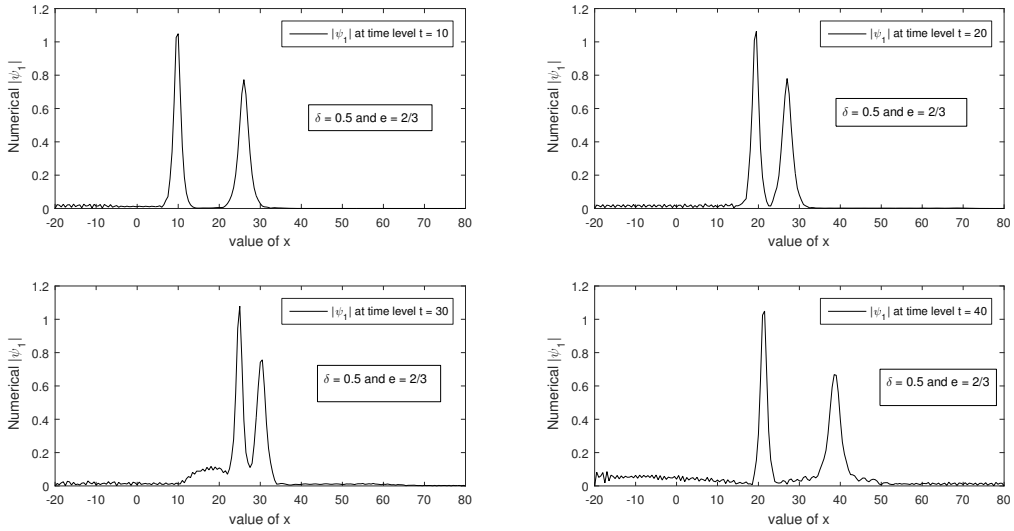

FIGURE 11. The numerical value of $|\Psi_1|$ or $|u|$ for $N = 201$, $\delta = 0.5$, e =2/3, $\alpha_1 = 1$, $\alpha_2 = 0.5$, $\nu_1 = 1$, $\nu_2 = 0.1$, and $\Delta t = 0.05$ at $t = 10$, 20, 30, and 40, respectively, regarding Example 3.2.

$$v(x,0) = \sqrt{\frac{2\alpha_1}{1+\epsilon}}\,\mathrm{sech}\left(\sqrt{2\alpha_1}\,x_1\right)\exp\left(i(\nu_1+\delta)x_1\right) + \sqrt{\frac{2\alpha_2}{1+\epsilon}}\,\mathrm{sech}\left(\sqrt{2\alpha_2}\,x_2\right)\exp\left(i(\nu_2+\delta)x_2\right) + \sqrt{\frac{2\alpha_3}{1+\epsilon}}\,\mathrm{sech}\left(\sqrt{2\alpha_3}\,x_3\right)\exp\left(i(\nu_3+\delta)x_3\right). \tag{3.14}$$

In the present example, elaboration regarding the elasticity of three solitons' interaction is provided. In Table 11, the first conserved quantities are compared with [26] at different values of t for $e = 2/3$ and $e = 1$, respectively. In Table 12, L_∞ error norms for first and second wave amplitudes are provided at $t = 2$, 4, 6, 8, and 10, respectively,

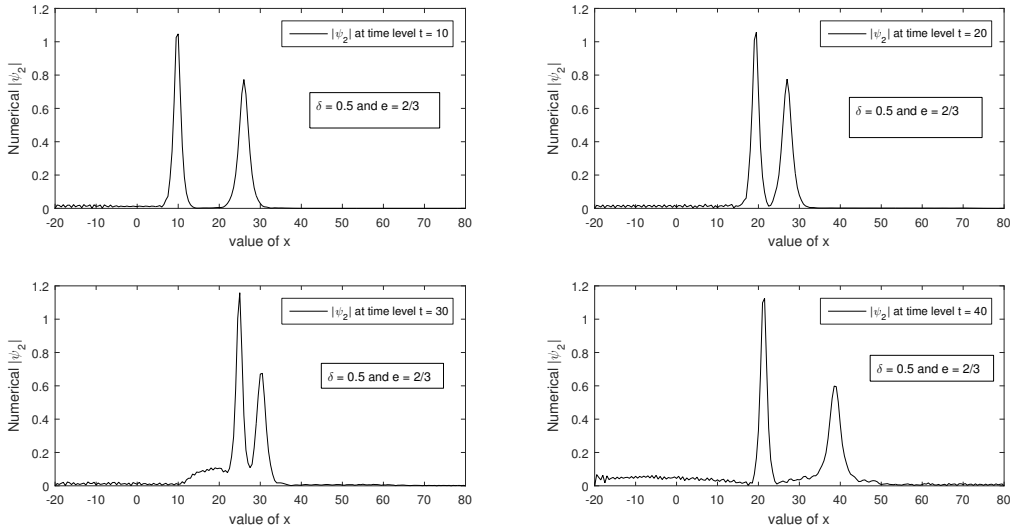

FIGURE 12. The numerical value of $|\Psi_2|$ or $|v|$ for $N = 201$, $\delta = 0.5$, e =2/3, $\alpha_1 = 1$, $\alpha_2 = 0.5$, $\nu_1 = 1$, $\nu_2 = 0.1$, and $\Delta t = 0.05$ at $t = 10$, 20, 30, and 40, respectively, regarding Example 3.2.

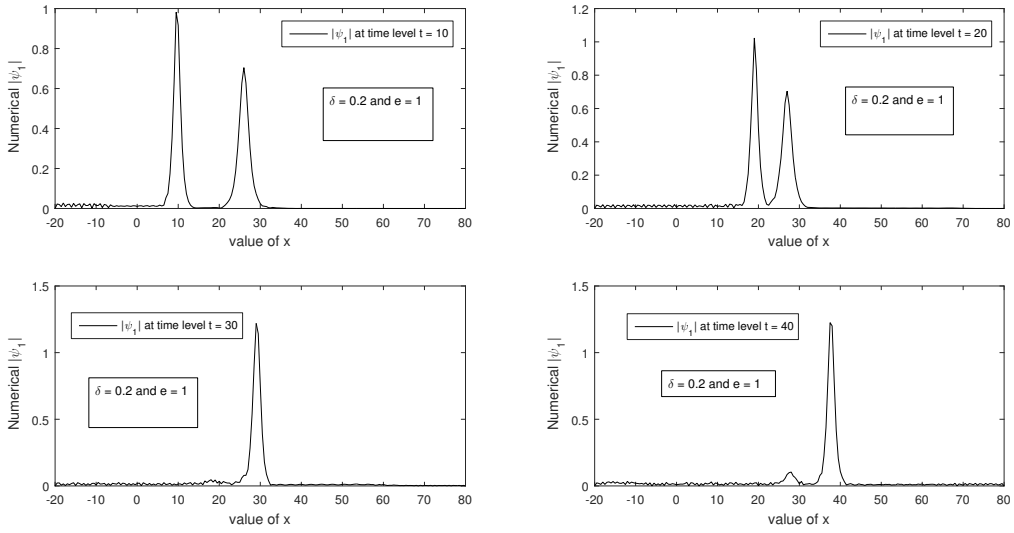

FIGURE 13. The numerical value of $|\Psi_1|$ or $|u|$ for $N = 201$, $\delta = 0.2$, $e = 1$, $\alpha_1 = 1$, $\alpha_2 = 0.5$, $\nu_1 = 1$, $\nu_2 = 0.1$, and $\Delta t = 0.05$ at $t = 10$, 20, 30, and 40, respectively, regarding Example 3.2.

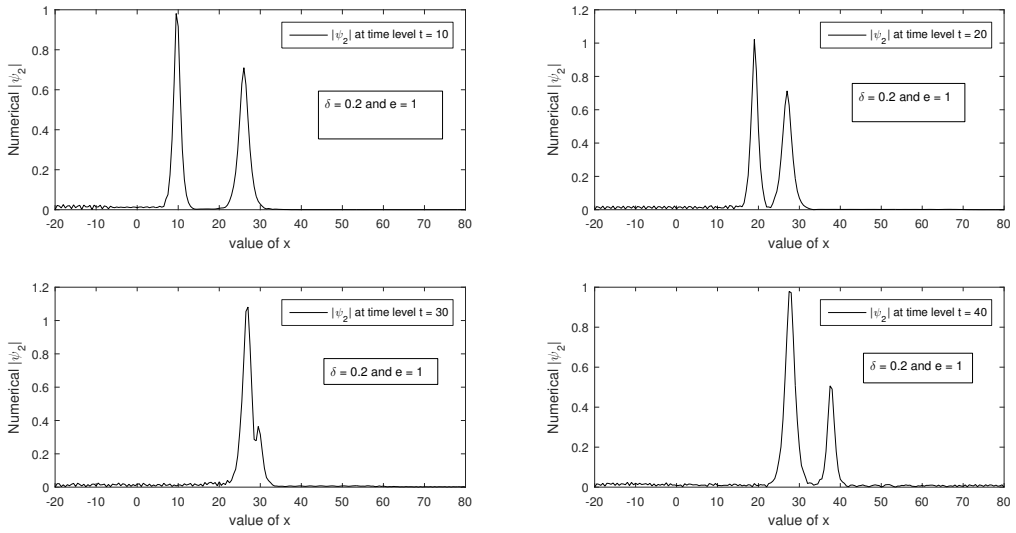

FIGURE 14. The numerical value of $|\Psi_2|$ or $|v|$ for $N = 201$, $\delta = 0.2$, $e = 1$, $\alpha_1 = 1$, $\alpha_2 = 0.5$, $\nu_1 = 1$, $\nu_2 = 0.1$, and $\Delta t = 0.05$ at $t = 10$, 20, 30, and 40, respectively, regarding Example 3.2.

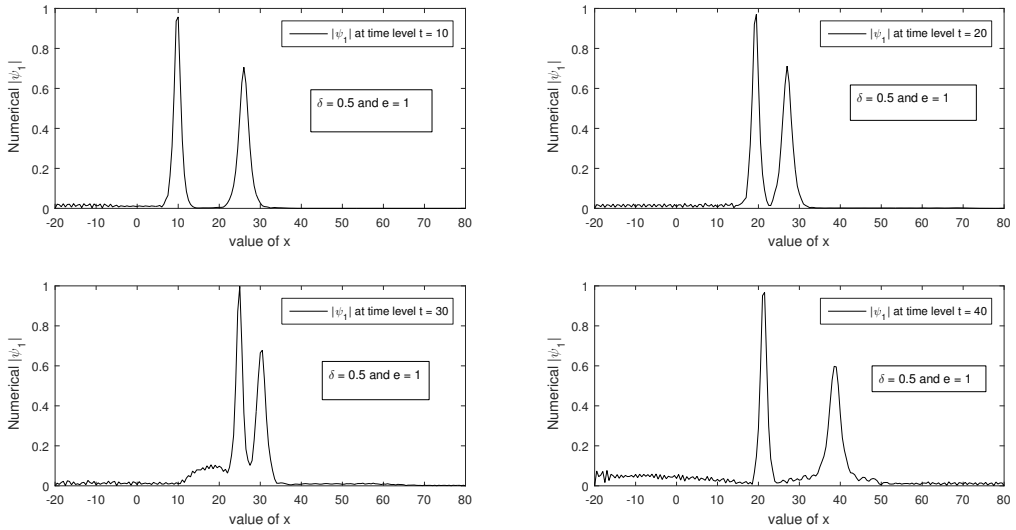

FIGURE 15. The numerical value of $|\Psi_1|$ or $|u|$ for $N = 201$, $\delta = 0.5$, $e = 1$, $\alpha_1 = 1$, $\alpha_2 = 0.5$, $\nu_1 = 1$, $\nu_2 = 0.1$, and $\Delta t = 0.05$ at $t = 10$, 20, 30, and 40, respectively, regarding Example 3.2.

for $\delta = 0.5$ and $e = 1$. In Figure 17, a graphical representation of the exact and numerical solutions for the first wave amplitude is provided at different time levels. In Figure 18, a graphical representation of exact and numerical solution for the second wave amplitude is given at different time levels. In Figures 17 and 18, it is observed that there is a good match between exact and numerical solutions, even if the time level is changed. In Figure 19, the three solitons' interaction for the first wave amplitude is shown. On changing the time level, all solitons moved from left to right without any disturbance in their shapes. This interaction is held at $\delta = 0.5$ and $e = 1$, since there is no change in the shapes of these solitons, so this interaction is an elastic interaction. In Figure 20, a graphical representation of three solitons' interaction for the second wave amplitude is shown; on changing the time levels, waves traveled from left to

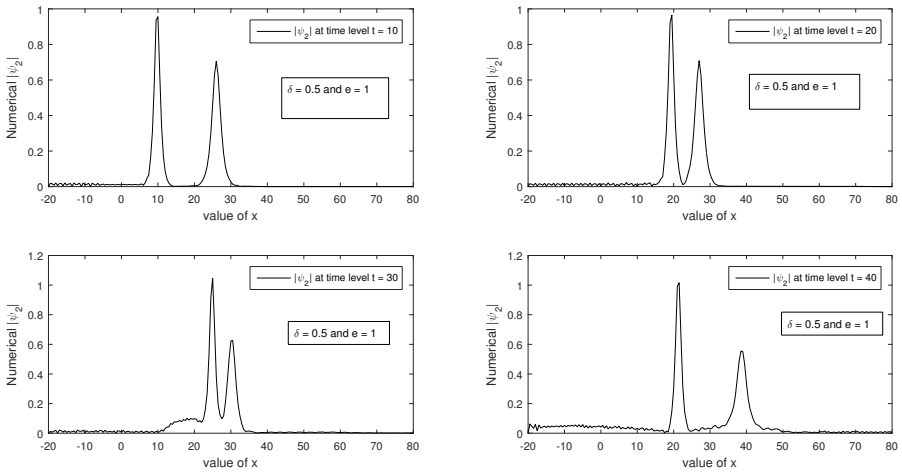

FIGURE 16. The numerical value of $|\Psi_2|$ or $|v|$ for $N = 201$, $\delta = 0.5$, $e = 1$, $\alpha_1 = 1$, $\alpha_2 = 0.5$, $\nu_1 = 1$, $\nu_2 = 0.1$, and $\Delta t = 0.05$ at $t = 10$, 20, 30, and 40, respectively, regarding Example 3.2.

right and maintained their shapes. This interaction was held at $\delta = 0.5$ and $e = 1$. This particular interaction is an elastic interaction since the shape of all waves got preserved during the interaction.

TABLE 11. Comparison of the conserved quantity for the interaction of three solitons for $\Delta t = 0.01$, $N = 301$, $\delta = 0.5$, $\alpha_1 = 1.2$, $\alpha_2 = 0.72$, $\alpha_3 = 0.36$, $\nu_1 = 1$, $\nu_2 = 0.1$, and $\nu_3 = -1$, for different values of ϵ regarding Example 3.3.

t	$\epsilon = \frac{2}{3}$		$\epsilon = 1$	
	I_1 [26]	I_1 [Present]	I_1 [26]	I_1 [Present]
10	2.077803	4.317252	1.896766	3.597710
20	2.077803	4.317238	1.896766	3.597698
30	2.077802	4.317181	1.896765	3.597652
40	2.077802	4.317477	1.896766	3.597870
50	2.077803	4.317540	1.896676	3.597909

TABLE 12. L_∞ error for the interaction of three solitons for $N = 301$, $\delta = 0.5$, $\alpha_1 = 1.2$, $\alpha_2 = 0.72$, $\alpha_3 = 0.36$, $\nu_1 = 1$, $\nu_2 = 0.1$, $\nu_3 = -1$, and $\epsilon = 1$ regarding Example 3.3.

t	$\Delta t = 0.01$		$\Delta t = 0.03$		$\Delta t = 0.05$	
	$L_\infty u$	$L_\infty v$	$L_\infty u$	$L_\infty v$	$L_\infty u$	$L_\infty v$
2	1.1252×10^{-6}	1.1247×10^{-6}	3.0174×10^{-5}	3.0166×10^{-5}	1.4059×10^{-4}	1.4056×10^{-4}
4	2.2755×10^{-6}	2.2876×10^{-6}	6.0859×10^{-5}	6.0857×10^{-5}	2.8117×10^{-4}	2.8116×10^{-4}
6	3.4501×10^{-6}	3.6460×10^{-6}	9.1463×10^{-5}	9.1591×10^{-5}	4.2111×10^{-4}	4.2116×10^{-4}
8	3.2011×10^{-6}	3.6208×10^{-6}	1.2032×10^{-4}	1.2063×10^{-4}	5.6011×10^{-4}	5.6031×10^{-4}
10	4.7234×10^{-6}	4.1296×10^{-6}	1.5131×10^{-4}	1.5056×10^{-4}	7.0029×10^{-4}	6.9937×10^{-4}

Example 3.4. In this example, $2D$ CNLS Eqs. (1.7) and (1.8) are given with the following initial conditions:

$$u(x, y, 0) = \lambda \operatorname{sech}(\beta_1 x + \beta_2 y) \exp\left[i\left\{-k_1 x - k_2 y\right\}\right], \tag{3.15}$$

$$v(x, y, 0) = \lambda \operatorname{sech}(\beta_1 x + \beta_2 y) \exp\left[i\left\{-k_1 x - k_2 y\right\}\right], \tag{3.16}$$

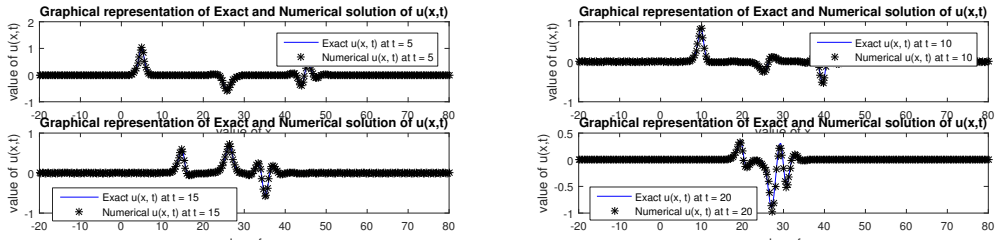

FIGURE 17. Graphical matching of exact and numerical solutions of first wave amplitude for $N = 301$, $\Delta t = 0.05$, $\delta = 0.5$, $\alpha_1 = 1.2$, $\alpha_2 = 0.72$, $\alpha_3 = 0.36$, $\nu_1 = 1$, $\nu_2 = 0.1$, $\nu_3 = -1$, and $e = 1$ at $t = 5$, 10, 15, and 20, respectively, in [-20, 80] regarding Example 3.3.

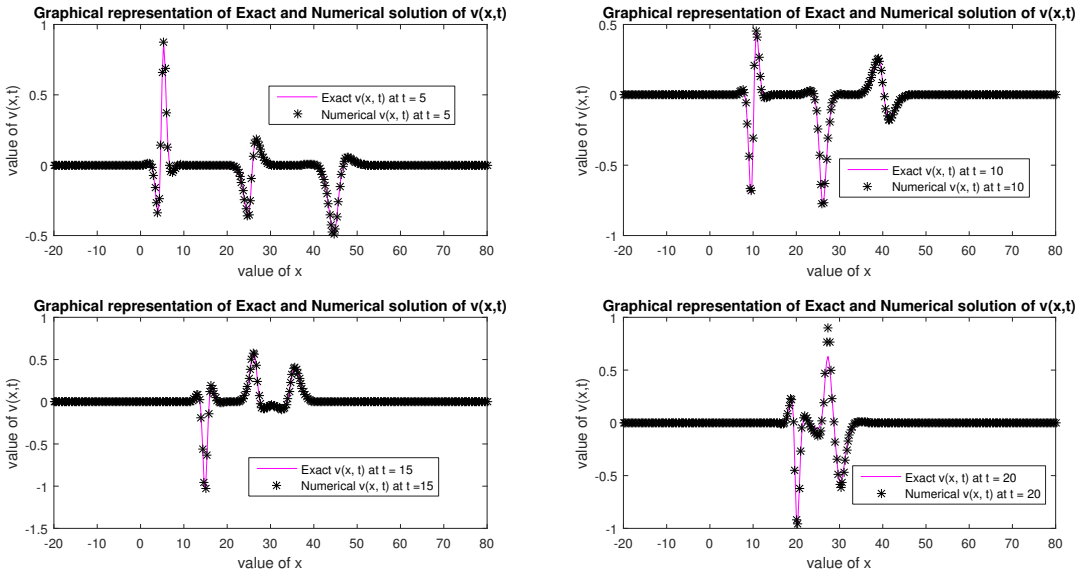

FIGURE 18. Graphical matching of exact and numerical solutions of second wave amplitude for $N = 301$, $\Delta t = 0.05$, $\delta = 0.5$, $\alpha_1 = 1.2$, $\alpha_2 = 0.72$, $\alpha_3 = 0.36$, $\nu_1 = 1$, $\nu_2 = 0.1$, $\nu_3 = -1$, and $e = 1$ at $t = 5, 10, 15$, and 20, respectively, in $[-20, 80]$ regarding Example 3.3.

where the computational domain is [-10, 10] and $\lambda = \sqrt{\frac{\beta_1^2+\beta_2^2}{1+\alpha}}$.

In the present example, no analytical solution is provided. In Figures 21 and 22, numerical solutions for first and second wave amplitudes are provided respectively at $t = 1$ for the different number of grid points.

4. Stability

By implementing the discretization formulae of the partial derivatives, in Eqs. (1.1) and (1.2), the following system of equations will be obtained.

$$\frac{du}{dt} = -\delta \sum_{j=1}^{N} a_{ij}^{(1)} u(x_j) + \frac{i}{2} \sum_{j=1}^{N} a_{ij}^{(2)} u(x_j) + i \left[|u|^2 + \epsilon |v|^2\right] u, \tag{4.1}$$

$$\frac{dv}{dt} = \delta \sum_{j=1}^{N} a_{ij}^{(1)} v(x_j) + \frac{i}{2} \sum_{j=1}^{N} a_{ij}^{(2)} v(x_j) + i \left[\epsilon |u|^2 + |v|^2\right] v. \tag{4.2}$$

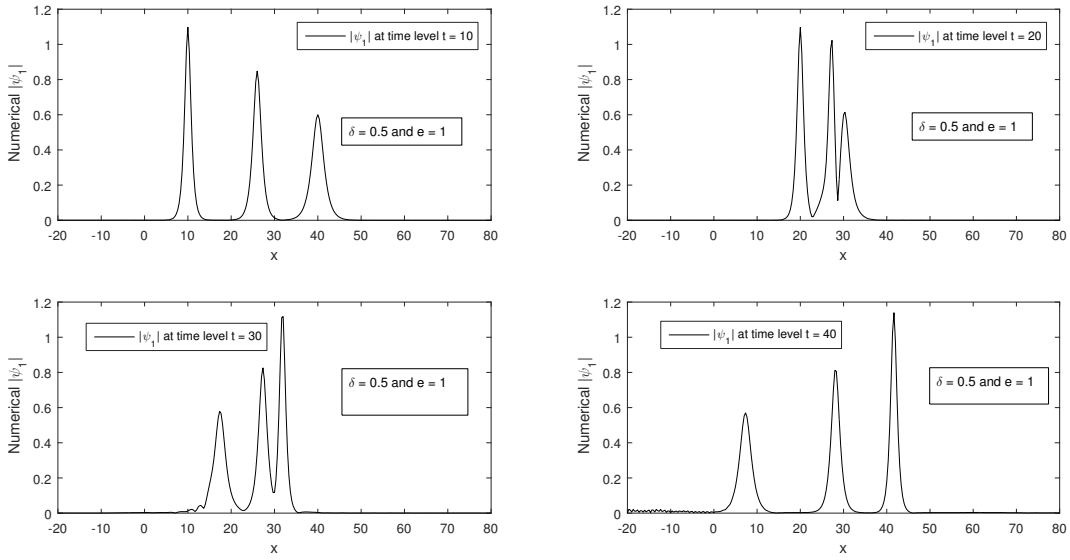

FIGURE 19. Graphical matching of numerical $|\Psi_1|$ or $|u|$ for $N = 301$, $\Delta t = 0.05$, $\delta = 0.5$, $\alpha_1 = 1.2$, $\alpha_2 = 0.72$, $\alpha_3 = 0.36$, $\nu_1 = 1$, $\nu_2 = 0.1$, $\nu_3 = -1$, and $e = 1$ at $t = 10$, 20, 30, and 40, respectively, in [-20, 80] regarding Example 3.3.

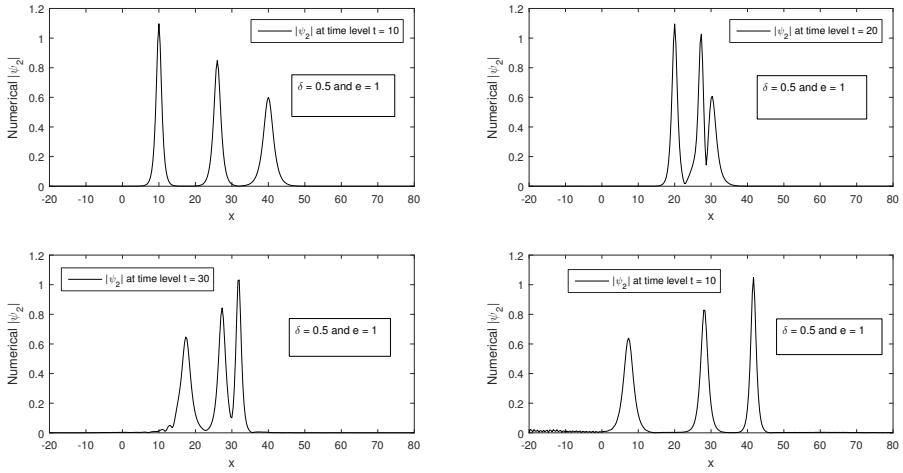

FIGURE 20. Graphical matching of numerical $|\Psi_2|$ or $|v|$ for $N = 301$, $\Delta t = 0.05$, $\delta = 0.5$, $\alpha_1 = 1.2$, $\alpha_2 = 0.72$, $\alpha_3 = 0.36$, $\nu_1 = 1$, $\nu_2 = 0.1$, $\nu_3 = -1$, $e = 1$ at $t = 10$, 20, 30 and 40 respectively in [-20, 80] regarding Example 3.3.

The above system of equations can be written as follows:

$$\begin{bmatrix} \frac{du}{dt} \\ \frac{dv}{dt} \end{bmatrix} = B_1 \begin{bmatrix} u \\ v \end{bmatrix} + f[u(x,t)], \tag{4.3}$$

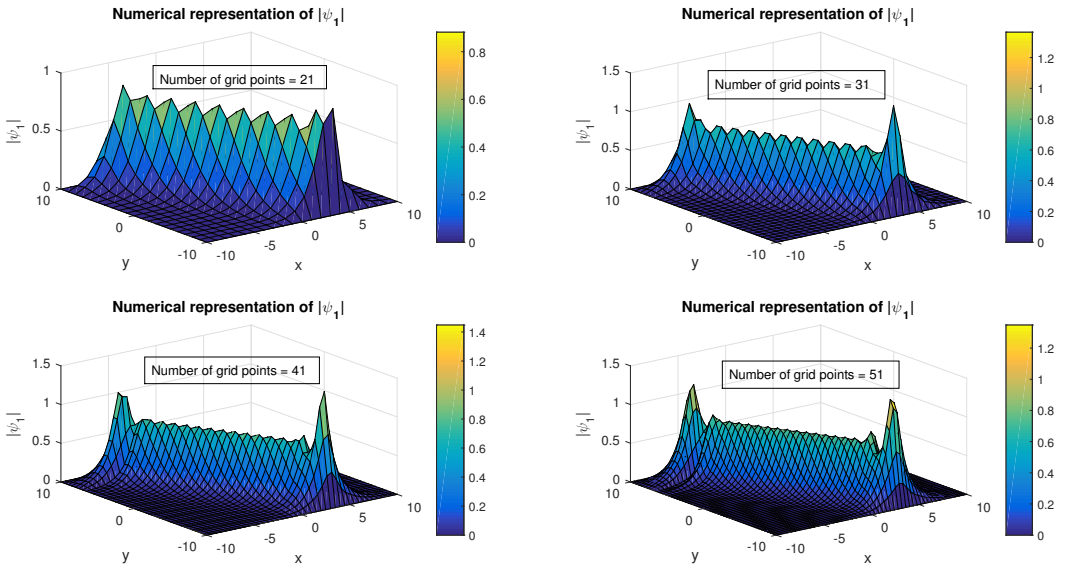

FIGURE 21. Numerical representation of $|\Psi_1|$ or $|u|$ for β_1=0.5,β_2=1,Δt=0.001,k_1=0.5,k_2=1 and α=1 at $t = 1$ regarding Example 3.4.

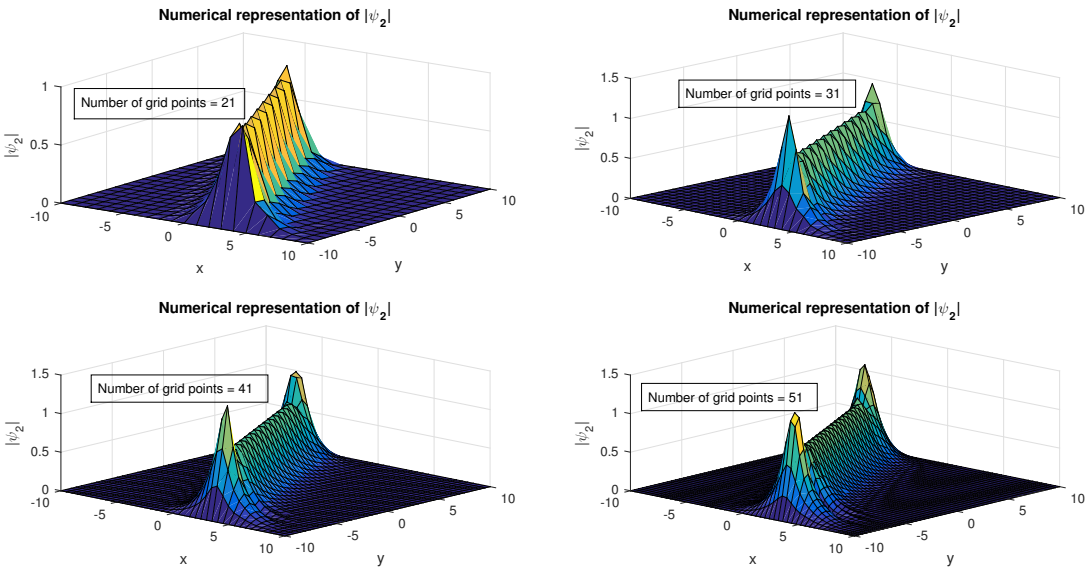

FIGURE 22. Numerical representation of $|\Psi_1|$ or $|u|$ for β_1=0.5,β_2=1,Δt=0.001,k_1=0.5,k_2=1 and α=1 at $t = 1$ regarding Example 3.4.

where matrix be is fetched from above-mentioned system of ODEs and $f[u(x,t)]$ is the corresponding nonlinear term. Stability of above system depends upon eigen values of matrix B_1.

$$B_1 = \begin{bmatrix} P_1 & O \\ O & P_2 \end{bmatrix},$$

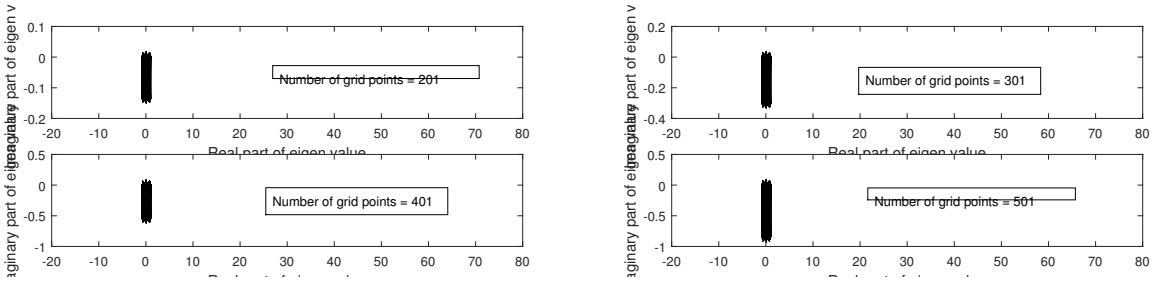

FIGURE 23. Stability of proposed scheme in one dimension at different number of grid points.

$$P_1 = \left[-\delta\, a_{ij}^{(1)} + \frac{i}{2} a_{ij}^{(2)}\right] \Delta t, \quad P_2 = \left[\delta\, a_{ij}^{(1)} + \frac{i}{2} a_{ij}^{(2)}\right] \Delta t.$$

Via discretization formula in the Eqs. (1.7) and (1.8) a newly formed system of ODEs will be obtained as follows:

$$\frac{du}{dt} = \frac{i}{2}\left[\sum_{j=1}^{N_1} b_{ij}\, u(x_j, y, t) + \sum_{j=1}^{N_2} b'_{ij}\, u(x, y_j, t)\right] + i\left[|u|^2 + \epsilon|v|^2\right] u, \tag{4.4}$$

$$\frac{dv}{dt} = \frac{i}{2}\left[\sum_{j=1}^{N_1} b_{ij}\, v(x_j, y, t) + \sum_{j=1}^{N_2} b'_{ij}\, v(x, y_j, t)\right] + i\left[\epsilon|u|^2 + \alpha|v|^2\right] v, \tag{4.5}$$

where above system of ODEs can be written as follows:

$$\begin{bmatrix} \frac{du}{dt} \\ \frac{dv}{dt} \end{bmatrix} = B_2 \begin{bmatrix} u \\ v \end{bmatrix} + g[u(x,t)]. \tag{4.6}$$

Stability of present scheme will depend upon eigenvalues of matrix B_2 and $g[u(x,t)]$ is corresponding nonlinear term.

$$B_2 = \begin{bmatrix} Q_1 & O \\ O & Q_2 \end{bmatrix},$$

$$Q_1 = \left[\frac{i}{2}\left(b_{ij} + b'_{ij}\right)\right] \Delta t, \quad Q_2 = \left[\frac{i}{2}\left(b_{ij} + b'_{ij}\right)\right] \Delta t.$$

Stability of proposed method is discussed via basic concepts [7][27]. By implementing matrix method for $1D$ and $2D$ CNLS equations, it can be assured that proposed scheme is stable and can be used to produce acceptable results. Figures 23 and 24 are provided regarding stability. Via Figure 25, the stability region for the proposed method is provided [6].

5. Conclusion

The coupled $1D$ and $2D$ Schrödinger equations are numerically approximated in current work using NUAH B-spline DQM. Shape-preserving qualities, which are essential for geometric modeling, are present in NUAH B-spline curves. Four numerical experiments are used to evaluate proposed scheme's effectiveness and correctness. Outcomes attained are flexible. Numerical and exact answers accord on problem well. Elasticity of soliton interactions is also investigated, and it is found that, depending on various values of δ and e, some interactions are elastic and non-elastic. This plan is simple to use and yields superior outcomes. Matrix stability analysis approach, which determines that the eigenvalues are found in the stable zone, also verifies the stability of suggested method.

Conflict of Interest: Authors have no conflict of interest.

Data Availability Statement: All data is included within the manuscript.

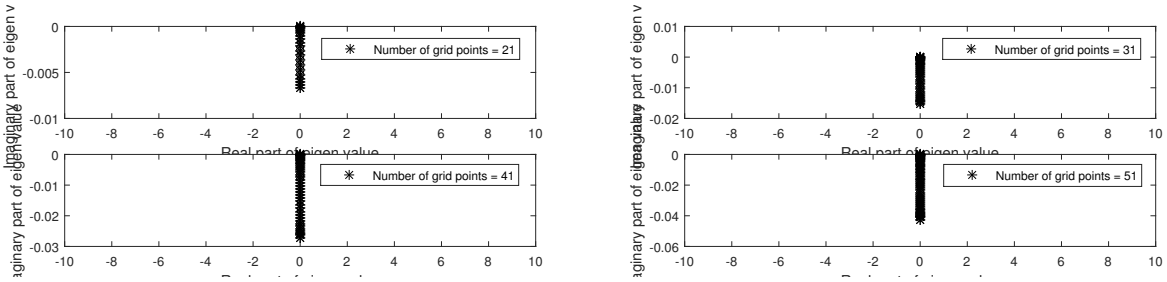

FIGURE 24. Stability of proposed scheme in two dimensions at different number of grid points.

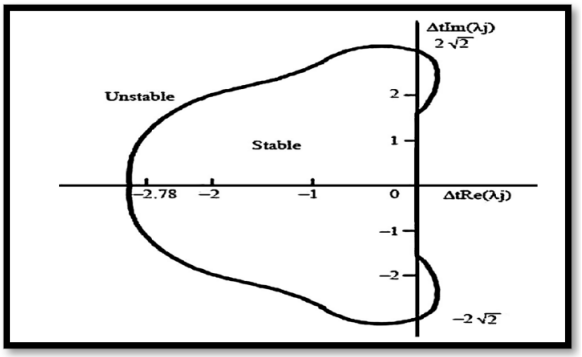

FIGURE 25. Stability region.

REFERENCES

[1] R. Abazari and R. Abazari, *Numerical study of some coupled PDEs by using differential transformation method*, In Proceedings of World Academy of Science, Engineering and Technology, *66* (2010, June), 52-59.

[2] M. J. Ablowitz and H. Segur, *Solitons and the inverse scattering transform*, Siam, *4* (1981).

[3] B. Ali, *An effective approximation to the dispersive soliton solutions of the coupled KdV equation via combination of two efficient methods*, [Journal details not provided].

[4] S. Alipour and F. Mirzaee, *An iterative algorithm for solving two-dimensional nonlinear stochastic integral equations: A combined successive approximations method with bilinear spline interpolation*, Applied Mathematics and Computation, *371* (2020), 124947.

[5] G. Arora and B. K. Singh, *Numerical solution of Burgers' equation with modified cubic B-spline differential quadrature method*, Applied Mathematics and Computation, *224* (2013), 166-177.

[6] G. Arora and V. Joshi, *A computational approach using modified trigonometric cubic B-spline for numerical solution of Burgers' equation in one and two dimensions*, Alexandria Engineering Journal, *57*(2) (2018), 1087-1098.

[7] G. Arora, V. Joshi, and R. C. Mittal, *Numerical Simulation of Nonlinear Schrödinger Equation in One and Two Dimensions*, Mathematical Models and Computer Simulations, *11*(4) (2019), 634-648.

[8] A. Aydin and B. Karasözen, *Multi-symplectic integration of coupled non-linear Schrödinger system with soliton solutions*, International Journal of Computer Mathematics, *86*(5) (2009), 864-882.

[9] A. Başhan, *A mixed methods approach to Schrödinger equation: Finite difference method and quartic B-spline based differential quadrature method*, An International Journal of Optimization and Control: Theories & Applications (IJOCTA), *9*(2) (2019), 223-235.

[10] A. Başhan, *A novel approach via mixed Crank–Nicolson scheme and differential quadrature method for numerical solutions of solitons of mKdV equation*, Pramana, *92*(6) (2019), 84.
[11] A. Başhan and N. M. Yağmurlu, *A mixed method approach to the solitary wave, undular bore and boundary-forced solutions of the Regularized Long Wave equation*, Computational and Applied Mathematics, *41*(4) (2022), 169.
[12] A. Bashan, N. M. Yağmurlu, Y. Uçar, and A. Esen, *An effective approach to numerical soliton solutions for the Schrödinger equation via modified cubic B-spline differential quadrature method*, Chaos, Solitons & Fractals, *100* (2017), 45-56.
[13] A. Başhan, Y. Uçar, N. M. Yağmurlu, and A. Esen, *Numerical solution of the complex modified Korteweg-de Vries equation by DQM*, In Journal of Physics: Conference Series, *766*(1) (2016, October), 012028, IOP Publishing.
[14] A. Başhan, Y. Uçar, N. M. Yağmurlu, and A. Esen, *A new perspective for quintic B-spline based Crank-Nicolson-differential quadrature method algorithm for numerical solutions of the nonlinear Schrödinger equation*, The European Physical Journal Plus, *133*(1) (2018), 12.
[15] R. Bellman, B. G. Kashef, and J. Casti, *Differential quadrature: a technique for the rapid solution of nonlinear partial differential equations*, Journal of Computational Physics, *10*(1) (1972), 40-52.
[16] J. Cao and G. Z. Wang, *Non-uniform B-spline curves with multiple shape parameters*, Journal of Zhejiang University Science C, *12*(10) (2011), 800.
[17] M. Dehghan, M. Abbaszadeh, and A. Mohebbi, *Numerical solution of system of N-coupled nonlinear Schrödinger equations via two variants of the meshless local Petrov-Galerkin (MLPG) method*, Comput. Model. Eng. Sci, *100*(5) (2014), 399-444.
[18] M. E. Fang and G. Wang, *ωB-splines*, Science in China Series F: Information Sciences, *51*(8) (2008), 1167-1176.
[19] Z. Gao, S. Song, and J. Duan, *The application of (2+1)-dimensional coupled nonlinear Schrödinger equations with variable coefficients in optical fibers*, Optik, *172* (2018), 953-967.
[20] S. Hajji, B. Danouj, and A. Lamnii, *UAT B-Splines of Order 4 for Reconstructing the Curves and Surfaces*, Applied Mathematical Sciences, *12*(21) (2018), 1007-1020.
[21] A. Hasegawa, *Optical solitons in fibers*, In Optical Solitons in Fibers, Springer, Berlin, Heidelberg, *1* (1989), 1-74.
[22] M. S. Ismail, *A fourth-order explicit scheme for the coupled nonlinear Schrödinger equation*, Applied Mathematics and Computation, *196*(1) (2008), 273-284.
[23] M. S. Ismail, *Numerical solution of coupled nonlinear Schrödinger equation by Galerkin method*, Mathematics and Computers in Simulation, *78*(4) (2008), 532-547.
[24] M. S. Ismail, H. A. Ashi, and F. Al-Rakhemy, *ADI method for solving the two-dimensional coupled nonlinear Schrödinger equation*, In AIP Conference Proceedings, *1648*(1) (2015, March), 050008, AIP Publishing LLC.
[25] M. S. Ismail and T. R. Taha, *A linearly implicit conservative scheme for the coupled nonlinear Schrödinger equation*, Mathematics and Computers in Simulation, *74*(4-5) (2007), 302-311.
[26] M. S. Ismail and T. R. Taha, *Numerical simulation of coupled nonlinear Schrödinger equation*, Mathematics and Computers in Simulation, *56*(6) (2001), 547-562.
[27] M. K. Jain, *Numerical solution of differential equations*, 2nd ed., Wiley, New York, *1* (1983).
[28] R. Jiwari, R. C. Mittal, and K. K. Sharma, *A numerical scheme based on weighted average differential quadrature method for the numerical solution of Burgers' equation*, Applied Mathematics and Computation, *219*(12) (2013), 6680-6691.
[29] R. Jiwari, S. Pandit, and R. C. Mittal, *A differential quadrature algorithm for the numerical solution of the second-order one dimensional hyperbolic telegraph equation*, International Journal of Nonlinear Science, *13*(3) (2012), 259-266.
[30] R. Jiwari, S. Pandit, and R. C. Mittal, *A differential quadrature algorithm to solve the two dimensional linear hyperbolic telegraph equation with Dirichlet and Neumann boundary conditions*, Applied Mathematics and Computation, *218*(13) (2012), 7279-7294.
[31] R. Jiwari, S. Pandit, and R. C. Mittal, *Numerical simulation of two-dimensional sine-Gordon solitons by differential quadrature method*, Computer Physics Communications, *183*(3) (2012), 600-616.
[32] A. Korkmaz and I. Dağ, *A differential quadrature algorithm for simulations of nonlinear Schrödinger equation*, Computers & Mathematics with Applications, *56*(9) (2008), 2222-2234.

[33] A. Korkmaz and I. Dağ, *Cubic B-spline differential quadrature methods for the advection-diffusion equation*, International Journal of Numerical Methods for Heat & Fluid Flow, *22*(8) (2012), 1021-1036.
[34] A. Korkmaz and I. Dağ, *Shock wave simulations using sinc differential quadrature method*, Engineering Computations, *28*(6) (2011), 654-674.
[35] A. Korkmaz and I. Dağ, *Solitary wave simulations of complex modified Korteweg–de Vries equation using differential quadrature method*, Computer Physics Communications, *180*(9) (2009), 1516-1523.
[36] B. I. Kvasov, *GB-splines and their properties*, International Journal of Annals of Numerical Mathematics, *3* (1996), 139-149.
[37] A. Lamnii, F. Oumellal, and J. Dabounou, *Tension Quartic Trigonometric Bézier Curves Preserving Interpolation Curves Shape*, International Journal of Mathematical Modelling & Computations, *5*(2) (2015), 99-109.
[38] Y. Lü, G. Wang, and X. Yang, *Uniform hyperbolic polynomial B-spline curves*, Computer Aided Geometric Design, *19*(6) (2002), 379-393.
[39] F. Mirzaee and S. Alipour, *A hybrid approach of nonlinear partial mixed integro-differential equations of fractional order*, Iranian Journal of Science and Technology, Transactions A: Science, *44*(3) (2020), 725-737.
[40] F. Mirzaee and S. Alipour, *An efficient cubic B-spline and bicubic B-spline collocation method for numerical solutions of multidimensional nonlinear stochastic quadratic integral equations*, Mathematical Methods in the Applied Sciences, *43*(1) (2020), 384-397.
[41] F. Mirzaee and S. Alipour, *Bicubic B-spline functions to solve linear two-dimensional weakly singular stochastic integral equation*, Iranian Journal of Science and Technology, Transactions A: Science, *45*(3) (2021), 965-972.
[42] F. Mirzaee and S. Alipour, *Cubic B-spline approximation for linear stochastic integro-differential equation of fractional order*, Journal of Computational and Applied Mathematics, *366* (2020), 112440.
[43] F. Mirzaee and S. Alipour, *Quintic B-spline collocation method to solve n-dimensional stochastic Itô-Volterra integral equations*, Journal of Computational and Applied Mathematics, *384* (2021), 113153.
[44] F. Mirzaee, S. Alipour, and N. Samadyar, *A numerical approach for solving weakly singular partial integro-differential equations via two-dimensional-orthonormal Bernstein polynomials with the convergence analysis*, Numerical Methods for Partial Differential Equations, *35*(2) (2019), 615-637.
[45] R. C. Mittal and R. Bhatia, *A numerical study of two dimensional hyperbolic telegraph equation by modified B-spline differential quadrature method*, Applied Mathematics and Computation, *244* (2014), 976-997.
[46] R. C. Mittal and R. Rohila, *Numerical simulation of reaction-diffusion systems by modified cubic B-spline differential quadrature method*, Chaos, Solitons & Fractals, *92* (2016), 9-19.
[47] R. C. Mittal and S. Dahiya, *A comparative study of modified cubic B-spline differential quadrature methods for a class of nonlinear viscous wave equations*, Engineering Computations, *35*(1) (2018), 315-333.
[48] R. C. Mittal and S. Dahiya, *Numerical simulation of three-dimensional telegraphic equation using cubic B-spline differential quadrature method*, Applied Mathematics and Computation, *313* (2017), 442-452.
[49] R. C. Mittal and S. Dahiya, *Numerical simulation on hyperbolic diffusion equations using modified cubic B-spline differential quadrature methods*, Computers & Mathematics with Applications, *70*(5) (2015), 737-749.
[50] H. Pottmann and M. G. Wagner, *Helix splines as an example of affine Tchebycheffian splines*, Advances in Computational Mathematics, *2*(1) (1994), 123-142.
[51] J. Qian and Y. Tang, *On non-uniform Algebraic-Hyperbolic (NUAH) B-splines*, Numerical Mathematics, *15*(4) (2006), 320.
[52] J. R. Quan and C. T. Chang, *New insights in solving distributed system equations by the quadrature method-I. Analysis*, Computers & Chemical Engineering, *13*(7) (1989), 779-788.
[53] J. R. Quan and C. T. Chang, *New insights in solving distributed system equations by the quadrature method-II. Numerical experiments*, Computers & Chemical Engineering, *13*(9) (1989), 1017-1024.
[54] W. Shen and G. Wang, *Changeable degree spline basis functions*, Journal of Computational and Applied Mathematics, *234*(8) (2010), 2516-2529.
[55] C. Shu, *Differential quadrature and its application in engineering*, Springer Science & Business Media, *1* (2012).
[56] C. Shu, *Generalized differential-integral quadrature and application to the simulation of incompressible viscous flows including parallel computation*, (Doctoral dissertation, ProQuest Dissertations & Theses) (1991).

[57] C. Shu and B. E. Richards, *High resolution of natural convection in a square cavity by generalized differential quadrature*, In Proceedings of the 3rd international conference on advances in numeric methods in engineering: theory and application, Swansea, UK, *1* (1990, January), 978-985.
[58] C. Shu and H. Xue, *Explicit computation of weighting coefficients in the harmonic differential quadrature*, Journal of Sound and Vibration, *204*(3) (1997), 549-555.
[59] H. S. Shukla, M. Tamsir, R. Jiwari, and V. K. Srivastava, *A numerical algorithm for computation modelling of 3D nonlinear wave equations based on exponential modified cubic B-spline differential quadrature method*, International Journal of Computer Mathematics, *95*(4) (2018), 752-766.
[60] W. J. Sonnier and C. I. Christov, *Strong coupling of Schrödinger equations: Conservative scheme approach*, Mathematics and Computers in Simulation, *69*(5-6) (2005), 514-525.
[61] A. G. Striz, X. Wang, and C. W. Bert, *Harmonic differential quadrature method and applications to analysis of structural components*, Acta Mechanica, *111*(1-2) (1995), 85-94.
[62] J. Q. Sun and M. Z. Qin, *Multi-symplectic methods for the coupled 1D nonlinear Schrödinger system*, Computer Physics Communications, *155*(3) (2003), 221-235.
[63] J. Q. Sun, X. Y. Gu, and Z. Q. Ma, *Numerical study of the soliton waves of the coupled nonlinear Schrödinger system*, Physica D: Nonlinear Phenomena, *196*(3-4) (2004), 311-328.
[64] N. H. Sweilam and R. F. Al-Bar, *Variational iteration method for coupled nonlinear Schrödinger equations*, Computers & Mathematics with Applications, *54*(7-8) (2007), 993-999.
[65] S. Tomasiello, *Numerical solutions of the Burgers–Huxley equation by the IDQ method*, International Journal of Computer Mathematics, *87*(1) (2010), 129-140.
[66] M. Wadati, T. Iizuka, and M. Hisakado, *A coupled nonlinear Schrödinger equation and optical solitons*, Journal of the Physical Society of Japan, *61*(7) (1992), 2241-2245.
[67] H. Wang, *Numerical studies on the split-step finite difference method for nonlinear Schrödinger equations*, Applied Mathematics and Computation, *170*(1) (2005), 17-35.
[68] G. Wang, Q. Chen, and M. Zhou, *NUAT B-spline curves*, Computer Aided Geometric Design, *21*(2) (2004), 193-205.
[69] Y. W. Wei and G. Z. Wang, *An orthogonal basis for non-uniform algebraic-trigonometric spline space*, Applied Mathematics-A Journal of Chinese Universities, *29*(3) (2014), 273-282.
[70] W. X. Wu, C. Shu, and C. M. Wang, *Vibration analysis of arbitrarily shaped membranes using local radial basis function-based differential quadrature method*, Journal of Sound and Vibration, *306*(1-2) (2007), 252-270.
[71] J. Xie and J. Tan, *Quasi-Cubic B-Spline Curves by Trigonometric Polynomials*, Journal of Information & Computational Science, *7*(6) (2010), 1215-1221.
[72] Y. Xu and C. W. Shu, *Local discontinuous Galerkin methods for nonlinear Schrödinger equations*, Journal of Computational Physics, *205*(1) (2005), 72-97.
[73] G. Xu and G. Z. Wang, *AHT Bézier curves and NUAHT B-spline curves*, Journal of Computer Science and Technology, *22*(4) (2007), 597-607.
[74] G. Xu and G. Z. Wang, *Extended cubic uniform B-spline and α-B-spline*, Acta Automatica Sinica, *34*(8) (2008), 980-984.
[75] J. Yang, *Multisoliton perturbation theory for the Manakov equations and its applications to nonlinear optics*, Physical Review E, *59*(2) (1999), 2393.
[76] J. Zhang, *C-curves: an extension of cubic curves*, Computer Aided Geometric Design, *13*(3) (1996), 199-217.
[77] J. Zhang, *Two different forms of CB-splines*, Computer Aided Geometric Design, *14*(1) (1997), 31-41.
[78] H. Q. Zhang, X. H. Meng, T. Xu, L. L. Li, and B. Tian, *Interactions of bright solitons for the (2+1)-dimensional coupled nonlinear Schrödinger equations from optical fibres with symbolic computation*, Physica Scripta, *75*(4) (2007), 537.